Journal of Directed Energy, **3**, Summer 2010, 349–383

Elemental Theory of a Relativistic Magnetron Operation: Anode Current

Andrey D. Andreev* **and Kyle J. Hendricks**

High-Power Microwave Division, Directed Energy Directorate, Air Force Research Laboratory, 3550 Aberdeen Avenue, Kirtland Air Force Base, New Mexico 87117-5776

and

Mikhail I. Fuks and Edl Schamiloglu

Department of Electrical and Computer Engineering, University of New Mexico, Albuquerque, New Mexico 87131-1356

The analytical expression allowing one to calculate the anode current of a relativistic magnetron is derived. The anode current is described as a cathode-to-anode drift of electron guiding centers in crossed external dc and induced rf (radio frequency) electric and magnetic fields along equipotential lines forming a magnetron spoke. The drift velocity of the electron guiding centers is calculated in the frame of reference moving with the phase velocity of the traveling rf wave associated with the induced rf electromagnetic field. Electron charge density near the cathode is considered as a parameter determining the electron guiding center charge density within the magnetron spoke. Anode current is calculated as a product of the electron guiding center cathode-to-anode drift velocity, the electron guiding center space charge density within the magnetron spoke, and the number of magnetron spokes. Results of the analytical calculations of the anode current of the A6 relativistic magnetron are compared with computer PIC simulations of the anode current of this magnetron.

KEYWORDS: Anode current, Drift in crossed $E \times H$ fields, Electron-guiding centers, Relativistic magnetron

1. Introduction

"The relativistic magnetron ... is one of the most mature of all high-power sources. The operational mechanism is robust; it is a relatively compact source; and it has been operated in the frequency range from just below 1 to about 10 GHz."[6] The first operational device of this kind was designed, built, and tested by Bekefi in the mid-1970s.[2,3,25,26] Since this seminal event, more than a dozen relativistic magnetrons have been reported as being operational and capable to generate high-power microwaves. The brief technical summaries and operational characteristics of most prominent relativistic magnetrons can be found elsewhere.[1,4-6,18,23,38]

Received January 12, 2010; revision received April 19, 2010.
*Corresponding author; e-mail: andreev@ece.unm.edu.

Theoretical analysis of a relativistic magnetron operation has always been connected with a well-developed theory of a nonrelativistic unstrapped magnetron summarized in a few classical[11,15,16,24,27,37,39] and many contemporary books. The very first attempt to derive more or less simple formulas allowing one to analytically calculate anode current and radiation power of a *relativistic* magnetron given its geometrical (cathode r_k, anode r_a, and vane r_v radii), operational (frequency f and mode of microwave oscillations determined by number of magnetron spokes n), and input (crossed external dc electric E_0 and magnetic H_0 fields) parameters was published by Nechaev et al.[21,22] at the end of the 1970s. This attempt is a direct extrapolation of a formulation by Kapitsa in the 1950s[16] and further explored by Nechaev in the beginning of the 1960s[19,20] as an analysis of operation of nonrelativistic magnetron-type devices. The analysis utilizes a simplified two-dimensional planar model of a cylindrical nonrelativistic multicavity magnetron, neglects electron space charge affecting electron motion between the cathode and the anode, and takes into account only the first synchronous spatial harmonic of the induced rf electric field, whose phase velocity v_{rf} is close to the drift velocity v_{dc} of electrons in the crossed external dc electric and magnetic fields.

The main distinguishing feature of the Kapitsa–Nechaev approach is the "adiabatic"[19,20] approximation of the electron motion between the cathode and the anode, whereby the drift of the electron guiding centers alone, without cyclotron gyration of electrons in the external dc magnetic field H_0, is taken into account; this is known now as the electron-guiding-center model.[12,13] The difference between Kapitza's[16] and Nechaev's[19,20] approaches is that in the first case the magnetron operation is analyzed in the laboratory frame of reference (LFR) with the following averaging of obtained results over one cyclotron period, whereas in the second case—the moving frame of reference (MFR)—which moves with the phase velocity v_{rf}. One of the most important operational characteristics of magnetron operation, the magnetron spoke current I_s, is determined in Refs. 21 and 22 as a cathode-to-anode drift in the crossed external dc and induced rf electric and magnetic fields of those electron guiding centers that enter the formed magnetron spoke in the direction parallel to the cathode surface as secondary electrons [Ref. 21, p. 310, Eq. (5)]:

$$I_s \sim \sigma L(v_{dc-} + v_{dc+}), \tag{1}$$

where σ is the surface charge density of the electron guiding centers near the cathode, L is the cathode length, and v_{dc-} and v_{dc+} are the parallel-to-cathode drift velocities of the electron guiding centers, to the left and to the right of the magnetron spoke, respectively. The charge density of the electron guiding centers σ is determined using the space-charge limiting approximation that assumes zero external dc electric E_0 field on the cathode surface, i.e., total compensation of the E_0 field by space charge of an electron sheath formed near the cathode.

The more comprehensive guiding-center model of relativistic crossed-field devices was developed by Riyopoulos in the 1990s[28–35] on the basis of the same Kapitsa's electron guiding-center approach,[16] taking into account all additional effects accompanying the magnetron spoke formation by a slow rf wave traveling inside the crossed electrostatic and magnetostatic fields: electron sheath thickness near the cathode, space-charge effects, etc. The magnetron spoke current I_s is determined[32,33] as the rf-induced drift of the electron guiding centers from the electron sheath boundary to the anode with a steady-state velocity v_x, assuming that the charge density of the electron guiding centers within the magnetron

spoke equals the electron sheath charge density ρ_H:

$$I_s \sim \rho_H L \int_{y_1}^{y_2} v_x(y)dy, \tag{2}$$

where the integration limits (coordinates) y_1 and y_2 (along the azimuthal direction of a cylindrical magnetron or along the direction of the traveling rf wave propagation in a planar magnetron) determine the width of that part of the electron sheath, from which the electron guiding centers drift into the magnetron spoke.

This paper presents a detailed outline of the first, simplified theory of a relativistic magnetron operation,[21,22] which attempted to make a transition from the even earlier developed theories of nonrelativistic magnetrons[16,19,20] to their relativistic analogs. The analytical expression for calculation of anode current in a relativistic magnetron is derived using this simplified theory and applied for calculating the anode current of the "classical" Bekefi's A6 relativistic magnetron[2,3,25,26]: "Since the classic experiments on the so-called A6 magnetron,[26] which produced an unprecedented rf output power of 900 MW, the A6 magnetron configuration has become the prototype for the next generation of relativistic magnetrons."[9] It has been intensively studied both experimentally and numerically (see references in Ref. 9), and that is the reason why operational characteristics of that "classical" A6 magnetron are used here as an ideal data set being compared with results of the analytic theory. Results of the analytically calculated anode current are compared with computer PIC simulations of the A6 relativistic magnetron operating in the π mode. Given the fact that the analytic theory represents the 2D geometry of a relativistic magnetron without its axial dimensions, the PIC simulations are performed using the well-studied 2D MAGIC code.†

The paper is organized as follows. Formulation of both external dc and induced rf electric and magnetic fields affecting the electron motion and the electron guiding center drift in a relativistic magnetron is presented in Sec. 2. Results of the analytical calculations of the anode current and their comparisons with the anode current obtained in the PIC simulation of the A6 magnetron are presented in Sec. 3. Conclusion is in Sec. 4.

2. Simplified Theory of a Magnetron Operation

2.1. Electric and magnetic fields in the LFR

2.1.1. Planar multicavity magnetron geometry. In accordance with Kapitza's original approach to define the induced rf electric potential U (denoted hereafter by subscript $\sim$) affecting electron motion in a planatron (planar magnetron) (Fig. 1),[16] the first term ($m = 1$) of the Fourier expansion of a periodic function that describes the $U_\sim$ potential in such a way that the phase of the corresponding induced rf electric field $E_\sim$ differs by π radians in neighboring cavities is [Ref. 16, p. 20, Eq. (2.08)]

$$\begin{aligned} U_\sim &= \frac{4}{\pi}\frac{U_1}{g_\parallel h}\frac{\sin\left(\frac{g_\parallel h}{2}\right)}{\sinh(g_\perp D)}\sinh(g_\perp y)\cos(g_\parallel x)\sin(\omega t) \\ &= \frac{4}{\pi}\frac{E_1}{g_\parallel}\frac{\sin\left(\frac{g_\parallel h}{2}\right)}{\sinh(g_\perp D)}\sinh(g_\perp y)\cos(g_\parallel x)\sin(\omega t), \end{aligned} \tag{3}$$

†http://www.magictoolsuite.com/.

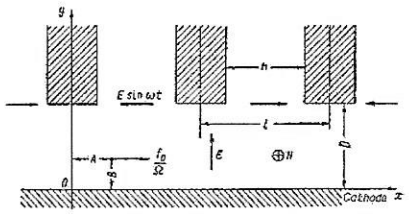

Fig 1. Kapitza's planatron (Ref. 16, p. 18, Fig. 1).

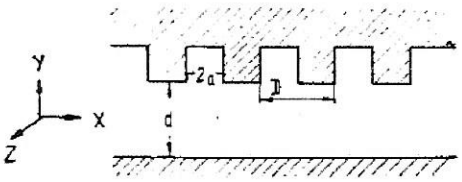

Fig. 2. Nechaev's "planar model of multi-cavity magnetron" (Ref. 19, p. 535, Fig. 1).

where $4/\pi$ is the appropriate Fourier expansion coefficient (Ref. 8, pp. 574–579), $\omega = 2\pi f$ is the angular frequency of the induced rf oscillations, U_1 and E_1 are the amplitudes of the induced rf potential $U_\sim$ and field $E_\sim$, respectively, which are the real functions of spatial coordinates x, y, and the time variable t,

$$E_1 = U_1/h, \tag{4}$$

h is the cavity width, D is the anode-cathode (AK) spacing, g is the wave number [Ref. 16, p. 19, Eq. (2.02)],

$$g = g_\perp = g_\parallel = \varphi/l = \pi/l, \tag{5}$$

and $\varphi = \pi$ is the phase variation of the $E_\sim$ field over a distance l— one spatial period of the planatron.

Analogous geometry of the original Nechajev's model of a multicavity magnetron (Fig. 2)[19] defines the width of one cavity h as $2a$, the spatial period l as D, and the AK spacing D as d, which allows one to rewrite Eq. (3) as [Ref. 19, p. 535, Eq. (2)]

$$U_\sim = \frac{2}{\pi}\frac{U_1}{g_\parallel a}\frac{\sin(g_\parallel a)}{\sinh(g_\perp d)}\sinh(g_\perp y)\cos(g_\parallel x)\sin(\omega t)$$

$$= \frac{4}{\pi}\frac{E_1}{g_\parallel}\frac{\sin(g_\parallel a)}{\sinh(g_\perp d)}\sinh(g_\perp y)\cos(g_\parallel x)\sin(\omega t), \tag{6}$$

where

$$E_1 = U_1/2a. \tag{7}$$

Both Kapitza's planatron (Fig. 1) and Nechajev's magnetron (Fig. 2) are immersed in the external dc electric E and magnetic H fields (denoted hereafter by subscript $\perp$) written using Nechajev's nomenclature of the multicavity magnetron geometry as (Fig. 2)

$$E_{\perp y} = E_0 = (U_0 - U_c)/d = V_0/d, \tag{8a}$$

$$H_{\perp z} = -H_0, \tag{8b}$$

where U_0 is the external dc potential applied to the anode, $U_c = 0$ is the potential of the cathode, and V_0 is, respectively, the AK voltage or the potential difference.

2.1.2. Nonrelativistic electric and magnetic fields. The induced rf electric field $E_\sim$ acting on an electron between the cathode and the anode has the following components [Ref. 16, p. 20, Eq. (2.09)]:

$$\begin{aligned} E_{\sim x} &= \frac{dU_\sim}{dx} = \frac{4}{\pi}\frac{E_1}{g_\parallel}\frac{\sin(g_\parallel a)}{\sinh(g_\perp d)}\sinh(g_\perp y)\frac{d\cos(g_\parallel x)}{dx}\sin(\omega t) \\ &= -\frac{4E_1}{\pi}\frac{\sin(g_\parallel a)}{\sinh(g_\perp d)}\sinh(g_\perp y)\sin(g_\parallel x)\sin(\omega t), \\ E_{\sim y} &= \frac{dU_\sim}{dy} = \frac{4}{\pi}\frac{E_1}{g_\parallel}\frac{\sin\left(\frac{g_\parallel h}{2}\right)}{\sinh(g_\perp D)}\frac{d\sinh(g_\perp y)}{dx}\cos(g_\parallel x)\sin(\omega t) \\ &= \frac{4E_1}{\pi}\frac{g_\perp}{g_\parallel}\frac{\sin(g_\parallel a)}{\sinh(g_\perp d)}\cosh(g_\perp y)\cos(g_\parallel x)\sin(\omega t). \end{aligned} \tag{9}$$

Rewriting Eqs. (9) as

$$\begin{aligned} E_{\sim x} &= -\frac{4E_1}{\pi}\frac{\sin(g_\parallel a)}{\sinh(g_\perp d)}\sinh(g_\perp y)\frac{\cos(g_\parallel x-\omega t)-\cos(g_\parallel x+\omega t)}{2}, \\ E_{\sim y} &= \frac{4E_1}{\pi}\frac{g_\perp}{g_\parallel}\frac{\sin(g_\parallel a)}{\sinh(g_\perp d)}\cosh(g_\perp y)\frac{\sin(g_\parallel x+\omega t)-\sin(g_\parallel x-\omega t)}{2} \end{aligned} \tag{10}$$

shows that the $E_\sim$ field (10) corresponds to a standing rf wave, which is the superposition of the two rf waves traveling one in the *negative-x* direction ($+\omega t$ term) and the other in the *positive-x* direction ($-\omega t$ term). By keeping in Eqs. (10) only one rf wave that travels in the *positive-x* direction and assuming that $g_\perp = g_\parallel$ [Eq. (5)] in the nonrelativistic case, one can obtain the $E_\sim$ field of this traveling in the *positive-x* direction the rf wave:

$$\begin{aligned} E_{\sim x} &= -\frac{2E_1}{\pi}\frac{\sin(g_\parallel a)}{\sinh(g_\perp d)}\sinh(g_\perp y)\cos(g_\parallel x-\omega t) = -E_{rf}\sinh(g_\perp y)\cos(g_\parallel x-\omega t), \\ E_{\sim y} &= -\frac{2E_1}{\pi}\frac{\sin(g_\parallel a)}{\sinh(g_\perp d)}\cosh(g_\perp y)\sin(g_\parallel x-\omega t) = -E_{rf}\cosh(g_\perp y)\sin(g_\parallel x-\omega t), \end{aligned} \tag{11}$$

where the E_{rf} amplitude is defined as [Ref. 19, p. 535, Eq. (4)]

$$E_{\mathrm{rf}} = \frac{2E_1}{\pi}\frac{\sin(g_\parallel a)}{\sinh(g_\perp d)} = \frac{U_1}{\pi a}\frac{\sin(g_\parallel a)}{\sinh(g_\perp d)} = \frac{U_1}{D\frac{\pi}{D}a}\frac{\sin(g_\parallel a)}{\sinh(g_\perp d)} = \frac{U_1}{D}\frac{\sin(g_\parallel a)}{g_\parallel a}\frac{1}{\sinh(g_\perp d)}. \tag{12}$$

The total electric E and magnetic H fields acting on an electron between the cathode and the anode of a nonrelativistic magnetron (Figs. 1 and 2) are determined as the superposition of the corresponding induced rf [Eqs. (11)] and external dc [Eqs. (8)] electric and magnetic

fields:

$$E_x = E_{\sim x} = -E_{\mathrm{rf}} \sinh(g_\perp y) \cos(g_\parallel x - \omega t), \tag{13a}$$

$$E_y = E_{\perp y} + E_{\sim y} = E_0 - E_{\mathrm{rf}} \cosh(g_\perp y) \sin(g_\parallel x - \omega t), \tag{13b}$$

$$H_z = H_{\perp z} = -H_0. \tag{13c}$$

2.1.3. Relativistic electric and magnetic fields. In a relativistic magnetron, the rf wave can travel along the cathode with any phase velocity υ_{rf}, which can be even relativistic in the general case; the latter means that the $E_\sim$ field [Eqs. (11)] of the rf wave traveling in the *positive-x* direction is to be written relativistically using relativistic factors γ_{rf} and β_{rf}:

$$\gamma_{\mathrm{rf}} = 1/\sqrt{1 - \beta_{\mathrm{rf}}^2}, \tag{14}$$

$$\beta_{\mathrm{rf}} = \upsilon_{\mathrm{rf}}/c = \sqrt{\frac{\gamma_{\mathrm{rf}}^2 - 1}{\gamma_{\mathrm{rf}}^2}}, \tag{15}$$

$$c = 1/\sqrt{\mu_0 \varepsilon_0}, \tag{16}$$

where μ_0 is the permeability, ε_0 is the permittivity, and c is the light speed.

To perform a transformation from the nonrelativistic $E_\sim$ field [Eqs. (11)] to its relativistic analog, two different frames of reference are defined. The first one, which moves with the velocity υ_{rf} [Eq. (15)] is the MFR, and the other one, which remains in rest, is the LFR. Notice that the induced rf electric field $E_\sim$ [Eqs. (11)] of the rf wave traveling in the same (as the MFR) *positive-x* direction with the same (as the MFR) velocity υ_{rf} (either relativistic or not) is uniquely defined in the MFR. Thus, the induced rf electric field $E_\sim$ in the LFR can be obtained by transformation of the $E_\sim$ field [Eqs. (11)] defined in the MFR (K' system) into the LFR (K system) using the following Lorentz relativistic transformation of electromagnetic field components [Ref. 17, p. 62, Eqs. (24.2) and (24.3)]:

$$\begin{pmatrix} E_x & H_x \\ E_y & H_y \\ E_z & H_z \end{pmatrix} = \begin{bmatrix} E'_x & H'_x \\ \gamma_{\mathrm{rf}}(E'_y + c\beta_{\mathrm{rf}}\mu_0 H'_z) & \gamma_{\mathrm{rf}}\left(H'_y - \beta_{\mathrm{rf}}\dfrac{E'_z}{c\mu_0}\right) \\ \gamma_{\mathrm{rf}}(E'_z - c\beta_{\mathrm{rf}}\mu_0 H'_y) & \gamma_{\mathrm{rf}}\left(H'_z + \beta_{\mathrm{rf}}\dfrac{E'_y}{c\mu_0}\right) \end{bmatrix}. \tag{17}$$

Substituting Eqs. (13) into Eq. (17) and replacing both transverse and longitudinal wave numbers $g_\perp$ and $g_\parallel$ [Eq. (5)] by the corresponding relativistic notations p and h gives both $E_\sim$ and $H_\sim$ fields, either relativistic or not, in the LFR:

$$E_{\sim x} = -E_{\mathrm{rf}} \sinh(py) \cos(hx - \omega t), \tag{18a}$$

$$E_{\sim y} = -\gamma_{\mathrm{rf}} E_{\mathrm{rf}} \cosh(py) \sin(hx - \omega t), \tag{18b}$$

$$H_{\sim z} = -\frac{\gamma_{\mathrm{rf}}\beta_{\mathrm{rf}}}{c\mu_0} E_{\mathrm{rf}} \cosh(py) \sin(hx - \omega t), \tag{18c}$$

where the E_{rf} amplitude [Eq. (12)] is defined as

$$E_{\mathrm{rf}} = \frac{2E_1}{\pi} \frac{\sin(ha)}{\sinh(pd)}. \tag{19}$$

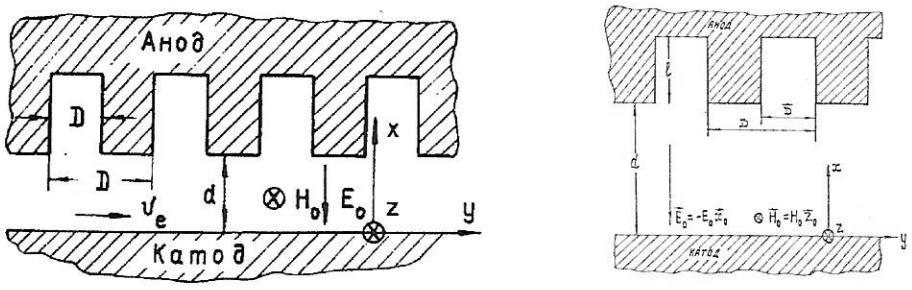

(a) (b)

Fig. 3. Planar model of a magnetron: (a) Ref. 22, p. 115, Fig. 1; and (b) Ref. 14, p. 288, Fig. 5.

In the nonrelativistic case, $\gamma_{\text{rf}} \to 1$ and $\beta_{\text{rf}} \to 0$, the $E_{\sim}$ fields [Eqs. (18a) and (18b)] transform to its nonrelativistic forms [Eqs. (11)] and the $H_{\sim}$ field [Eq. 18(c)] vanishes to zero.

Without any loss of generality with the previously defined geometry of the planar magnetron (Figs. 1 and 2), one can (i) place the cathode along the y axis and the AK spacing along the x axis and (ii) change directions and, hence, the sign of the $E_{\perp y}$ [Eqs. (8)] field (Fig. 3) and, respectively, both $E_{\sim y}$ and $E_{\sim x}$ fields into the opposite ones. After this transformation, the direction of the z axis changes into the opposite one, and, hence, both $H_{\perp z}$ and $H_{\sim z}$ fields change their signs (Fig. 3).

In the newly defined geometry of the planar magnetron (Fig. 3) the rf wave travels in the *positive-y* direction with phase velocity v_{rf} [Ref. 6, p. 262, Eq. (7.2), and Ref. 225, p. 114, Eq. (1)]:

$$v_{\text{rf}} = \omega/h, \tag{20}$$

where the longitudinal wave number h is defined as the phase variation $\varphi = \pi$ of the $E_{\sim}$ field ("π-mode-distribution" approximation) over one spatial period D [Eq. (5)]:

$$h = \pi/D. \tag{21}$$

The relation of the free-space wave number $k = \omega/c$ to the longitudinal wave number h [Eq. (21)] is

$$k/h = \omega/ch = v_{\text{rf}}/c = \beta_{\text{rf}}, \tag{22}$$

and the correlation between the transverse p, the longitudinal h [Eq. (21)], and the free-space k wave numbers is [Ref. 34, p. 1346, Eq. (9)]

$$p = \sqrt{h^2 - k^2} = \sqrt{\left(\frac{k}{\beta_{\text{rf}}}\right)^2 - k^2} = k\sqrt{\frac{1-\beta_{\text{rf}}^2}{\beta_{\text{rf}}^2}} = \frac{k}{\beta_{\text{rf}}}\sqrt{1-\beta_{\text{rf}}^2} = \frac{k}{\beta_{\text{rf}}\gamma_{\text{rf}}} = \frac{h}{\gamma_{\text{rf}}} = h'. \tag{23}$$

In the nonrelativistic case, $\gamma_{\text{rf}} \to 1$, the transverse wave number p [Eq. (23)] equals the longitudinal wave number h [Eq. (21)].

After making transformation from the x-direction-oriented cathode (Figs. 1 and 2) to the y-direction-oriented cathode (Fig. 3) and changing signs of both $E_{\sim}$ and $H_{\sim}$ fields into the opposite ones, the induced rf electric and magnetic fields [Eqs. (18)] (lettered hereafter as

EMF^{rf}) are written as [Ref. 14, p. 289, Eq. (12), and Ref. 34, p. 1346, Eqs. (6–11)]

$$\begin{aligned} E_{\sim y} &= E_{\text{rf}} \sinh(px)\cos(hy-\omega t), \\ E_{\sim x} &= \gamma_{\text{rf}} E_{\text{rf}} \cosh(px)\sin(hy-\omega t) = \frac{h}{p} E_{\text{rf}} \cosh(px)\sin(hy-\omega t), \\ H_{\sim z} &= \frac{\gamma_{\text{rf}}\beta_{\text{rf}}}{c\mu_0} E_{\text{rf}} \cosh(px)\sin(hy-\omega t) = \frac{1}{\sqrt{\mu_0/\varepsilon_0}} \frac{k}{p} E_{\text{rf}} \cosh(px)\sin(hy-\omega t), \end{aligned} \tag{24}$$

and both E_0 and H_0 fields (8) also change their signs into the opposite ones. The H_0 field is directed now along the z axis, and the E_0 field is directed from the anode to the cathode oppositely to the direction of the x axis. The external dc electric and magnetic fields [Eqs. (8)] (lettered hereafter as EMF^{dc}) are written as

$$E_{\perp x} = -E_0, \tag{25a}$$

$$H_{\perp z} = H_0. \tag{25b}$$

The total electric E and magnetic H fields (lettered hereafter as $\text{EMF}^{\text{rf/dc}}$) are defined as the superposition of the EMF^{rf} [Eqs. (24)] and the EMF^{dc} [Eqs. (25)]:

$$E_y = E_{\sim y} = E_{\text{rf}} \sinh(px)\cos(hy-\omega t), \tag{26a}$$

$$E_x = E_{\perp x} + E_{\sim x} = -E_0 + \gamma_{\text{rf}} E_{\text{rf}} \cosh(px)\sin(hy-\omega t), \tag{26b}$$

$$H_z = H_{\perp z} + H_{\sim z} = \frac{E_0}{c\beta_{\text{dc}}\mu_0} + \frac{1}{\sqrt{\mu_0/\varepsilon_0}} \beta_{\text{rf}}\gamma_{\text{rf}} E_{\text{rf}} \cosh(px)\sin(hy-\omega t). \tag{26c}$$

2.1.4. Electron motion in the LFR. In the absence of the EMF^{rf} [Eqs. (24)], i.e., when the E_1 amplitude [Eq. (7)] is zero, an electron moves in the EMF^{dc} [Eqs. (25)] only, along a trajectory, which is a superposition of (i) the electron drift along the cathode with the drift velocity υ_{dc},

$$\upsilon_{\text{dc}} = c\beta_{\text{dc}} = -\frac{1}{\mu_0}\frac{E_{\perp x}}{H_{\perp z}} = -\frac{1}{\mu_0}\frac{-E_0}{H_0} = \frac{E_0}{\mu_0 H_0}, \tag{27}$$

and (ii) the electron gyration in the plane perpendicular to the $H_{\perp z}$ field [Eq. (25b)] lines with the cyclotron frequency ω_c [Ref. 10, p. 18, Eqs. (2)–(3)] and the Larmor radius r_L [Ref. 10, p. 18, Eqs. (2)–(6), and Ref. 17, p. 53, Eq. (21.6)]:

$$\omega_c = \frac{|q_e|}{m_e}\mu_0 H_{\perp z} = \frac{|q_e|}{m_e}\mu_0 H_0 = \frac{|q_e|E_0}{m_e \upsilon_{\text{dc}}}, \tag{28}$$

$$r_L = \frac{\upsilon_0 + \upsilon_{\text{dc}}}{\omega_c} = \frac{(\upsilon_0 + \upsilon_{\text{dc}})m_e}{|q_e|\,\mu_0 H_0}, \tag{29}$$

where q_e and m_e are the electron charge and mass, respectively, and υ_0 is the "initial" velocity with which the cathode emits this electron. In the most common case, when the "initial" velocity υ_0 is much less than the drift velocity υ_{dc} [Eq. (27)], one can assume that $\upsilon_0 = 0$. The Larmor radius [Eq. (29)] of the gyrating electron is determined in this case as

$$r_L = \frac{\upsilon_{\text{dc}} m_e}{|q_e|\mu_0 H_0} = \frac{m_e E_0}{|q_e|\,(\mu_0 H_0)^2} = \frac{m_e E_0}{|q_e|\left(\dfrac{E_0}{c\beta_{\text{dc}}}\right)^2} = c^2\beta_{\text{dc}}^2 \frac{m_e}{|q_e|E_0}. \tag{30}$$

Synchronism between an electron drifting in the EMF^{dc} [Eqs. (25)] with the drift velocity v_{dc} [Eq. (27)] and the rf wave traveling in the same *positive-y* direction with the phase velocity v_{rf} [Eq. (20)] occurs when

$$v_{dc} = v_{rf}. \tag{31}$$

Detuning from exact synchronism [Eq. (31)] is described by the detuning coefficient α [Ref. 22, p. 116, and Ref. 14, p. 290, Eq. (15)]:

$$\alpha = 1 - \frac{v_{rf}}{v_{dc}} = 1 - \frac{\beta_{rf}}{\beta_{dc}}, \tag{32}$$

which can be either positive, when $\beta_{dc} > \beta_{rf}$, or negative, when $\beta_{dc} < \beta_{rf}$. In the first case, when $\alpha > 0$, an electron drifting in EMF^{dc} [Eqs. (25)] "would push on the wave as it moves uphill; then the wave could gain energy," whereas in the second case, when $\alpha < 0$, an electron drifting in EMF^{dc} [Eqs. (25)] "gains energy, and therefore the wave must lose energy and is damped" (Ref. 10, pp. 219–220, Figs. 7–17). One can say also that in the first case an "electron is giving up energy to rf field," whereas in the second case an "electron is absorbing energy from rf field" (Ref. 37, p. 311, Fig. 62).

The cyclotron gyration of electrons forms the electron sheath near the cathode, which is going to be a source (hub) of electrons drifting from the cathode toward the anode when conditions for this drift occur. The top boundary of the electron sheath x_b, called the "boundary line," is determined by the Larmor diameter or the doubled Larmor radius [Eq. (61)]:

$$x_b = 2r_L. \tag{33}$$

The starting position of the electron guiding centers drifting from the cathode toward the anode x_f, called the "feeding line" for the anode current, is determined as the Larmor radius [Eq. (61)]:

$$x_f = r_L. \tag{34}$$

When the E_1 amplitude [Eq. (7)] is sufficiently greater than zero, an electron moves in the $EMF^{rf/dc}$ [Eqs. (26)] along a trajectory, which is the superposition of (i) the electron drift in the crossed E_x [Eq. (26b)] and H_z [Eq. (26c)] fields, i.e., the $E_x \times H_z$ drift; (ii) the electron drift in the crossed E_y [Eq. (26a)] and H_z [Eq. (26c)] fields, i.e., the $E_y \times H_z$ drift; and (iii) the electron gyration in the plane perpendicular to the H_z [Eq. (26c)] field lines.

2.2. Electric and magnetic fields in the MFR

2.2.1. Induced rf electric and magnetic fields. The analytical analysis of an electron trajectory in the LFR is rather complicated because all components of the $EMF^{rf/dc}$ [Eqs. (26)] vary in both time and space due to their dependence on the induced rf electric field, as do velocities of both $E_x \times H_z$ and $E_y \times H_z$ drifts. The analysis is sufficiently simplified when transition is made from the LFR into the MFR that moves with the phase velocity v_{rf} [Eq. (20)]. Both EMF^{rf} [Eqs. (24)] and EMF^{dc} [Eqs. (25)] are transformed from the LFR (K system) to the v_{rf} moving with velocity [Eq. (20)] MFR (K' system) using the following Lorentz relativistic transformations of electromagnetic field components

[Ref. 17, p. 62, Eqs. (24.2) and (24.3)]:

$$\begin{pmatrix} E'_y & H'_y \\ E'_x & H'_x \\ E'_z & H'_z \end{pmatrix} = \begin{bmatrix} E_y & B_y \\ \gamma_{\mathrm{rf}}(E_x - c\beta_{\mathrm{rf}}\mu_0 H_z) & \gamma_{\mathrm{rf}}\left(H_x + \beta_{\mathrm{rf}}\dfrac{E_z}{c\mu_0}\right) \\ \gamma_{\mathrm{rf}}(E_z + c\beta_{\mathrm{rf}}\mu_0 H_x) & \gamma_{\mathrm{rf}}\left(H_z - \beta_{\mathrm{rf}}\dfrac{E_x}{c\mu_0}\right) \end{bmatrix}. \tag{35}$$

The relativistic transformation [Eq. (35)] is the reversed one to the transformation [Eq. (17)].

Substituting Eqs. (24) into Eq. (35) gives

$$\begin{aligned} E'_{\sim y} &= E_{\mathrm{rf}} \sinh(px)\cos(hy - \omega t), \\ E'_{\sim x} &= \gamma_{\mathrm{rf}}\left[\gamma_{\mathrm{rf}} E_{\mathrm{rf}} \cosh(px)\sin(hy - \omega t)\right. \\ &\quad \left. - c\beta_{\mathrm{rf}}\frac{\mu_0}{\sqrt{\mu_0/\varepsilon_0}}\beta_{\mathrm{rf}}\gamma_{\mathrm{rf}} E_{\mathrm{rf}} \cosh(px)\sin(hy - \omega t)\right], \\ H'_{\sim z} &= \gamma_{\mathrm{rf}}\left[\frac{\mu_0}{\sqrt{\mu_0/\varepsilon_0}}\beta_{\mathrm{rf}}\gamma_{\mathrm{rf}} E_{\mathrm{rf}} \cosh(px)\sin(hy - \omega t)\right. \\ &\quad \left. - \frac{\beta_{\mathrm{rf}}}{c}\gamma_{\mathrm{rf}} E_{\mathrm{rf}} \cosh(px)\sin(hy - \omega t)\right], \end{aligned} \tag{36}$$

or

$$\begin{aligned} E'_{\sim y} &= E_{\mathrm{rf}} \sinh(px)\cos(hy - \omega t), \\ E'_{\sim x} &= \gamma_{\mathrm{rf}}^2 E_{\mathrm{rf}}\left(1 - \beta_{\mathrm{rf}}^2\frac{c\mu_0}{\sqrt{\mu_0/\varepsilon_0}}\right)\cosh(px)\sin(hy - \omega t) \\ &= \gamma_{\mathrm{rf}}^2 E_{\mathrm{rf}}\left(1 - \beta_{\mathrm{rf}}^2\right)\cosh(px)\sin(hy - \omega t), \\ H'_{\sim z} &= \gamma_{\mathrm{rf}}^2\beta_{\mathrm{rf}} E_{\mathrm{rf}}\left(\frac{\mu_0}{\sqrt{\mu_0/\varepsilon_0}} - \frac{1}{c}\right)\cosh(px)\sin(hy - \omega t) = 0, \end{aligned} \tag{37}$$

or

$$\begin{aligned} E'_{\sim y} &= E_{\mathrm{rf}} \sinh(px)\cos(hy - \omega t), \\ E'_{\sim x} &= E_{\mathrm{rf}} \cosh(px)\sin(hy - \omega t), \\ H'_{\sim z} &= 0. \end{aligned} \tag{38}$$

It follows from Eqs. (38) that the $\mathrm{EMF}^{\mathrm{rf}}$ is purely electric (zero $H'_{\sim}$ field) and nonrelativistic; one can compare Eqs. (38) with Eqs. (11).

The time-dependent components of the $\mathrm{EMF}^{\mathrm{rf}}$ [Eqs. (38)], can be rewritten, using Eq. (22), as follows:

$$\begin{aligned} hy - \omega t &= \frac{h}{\gamma_{\mathrm{rf}}}\gamma_{\mathrm{rf}} y - \omega t = h'\gamma_{\mathrm{rf}} y - \omega t = h'\left(\gamma_{\mathrm{rf}} y - \frac{\omega}{h'}t\right) = h'\left(\gamma_{\mathrm{rf}} y - \frac{\omega\gamma_{\mathrm{rf}}}{h}t\right) \\ &= h'\gamma_{\mathrm{rf}}\left(y - \frac{\omega}{h}t\right) = h'\gamma_{\mathrm{rf}}(y - \upsilon_{\mathrm{rf}}t) = h'\gamma_{\mathrm{rf}}(y - \beta_{\mathrm{rf}}ct) = h'y', \end{aligned} \tag{39}$$

where

$$y' = \gamma_{\mathrm{rf}}(y - \beta_{\mathrm{rf}}ct). \tag{40}$$

[Ref. 17, p. 62, Eqs. (24.2) and (24.3)]:

$$\begin{pmatrix} E'_y & H'_y \\ E'_x & H'_x \\ E'_z & H'_z \end{pmatrix} = \begin{bmatrix} E_y & B_y \\ \gamma_{\rm rf}(E_x - c\beta_{\rm rf}\mu_0 H_z) & \gamma_{\rm rf}\left(H_x + \beta_{\rm rf}\dfrac{E_z}{c\mu_0}\right) \\ \gamma_{\rm rf}(E_z + c\beta_{\rm rf}\mu_0 H_x) & \gamma_{\rm rf}\left(H_z - \beta_{\rm rf}\dfrac{E_x}{c\mu_0}\right) \end{bmatrix}. \tag{35}$$

The relativistic transformation [Eq. (35)] is the reversed one to the transformation [Eq. (17)].

Substituting Eqs. (24) into Eq. (35) gives

$$\begin{aligned} E'_{\sim y} &= E_{\rm rf}\sinh(px)\cos(hy-\omega t), \\ E'_{\sim x} &= \gamma_{\rm rf}\left[\gamma_{\rm rf}E_{\rm rf}\cosh(px)\sin(hy-\omega t)\right. \\ &\quad \left. - c\beta_{\rm rf}\frac{\mu_0}{\sqrt{\mu_0/\varepsilon_0}}\beta_{\rm rf}\gamma_{\rm rf}E_{\rm rf}\cosh(px)\sin(hy-\omega t)\right], \\ H'_{\sim z} &= \gamma_{\rm rf}\left[\frac{\mu_0}{\sqrt{\mu_0/\varepsilon_0}}\beta_{\rm rf}\gamma_{\rm rf}E_{\rm rf}\cosh(px)\sin(hy-\omega t)\right. \\ &\quad \left. - \frac{\beta_{\rm rf}}{c}\gamma_{\rm rf}E_{\rm rf}\cosh(px)\sin(hy-\omega t)\right], \end{aligned} \tag{36}$$

or

$$\begin{aligned} E'_{\sim y} &= E_{\rm rf}\sinh(px)\cos(hy-\omega t), \\ E'_{\sim x} &= \gamma_{\rm rf}^2 E_{\rm rf}\left(1-\beta_{\rm rf}^2\frac{c\mu_0}{\sqrt{\mu_0/\varepsilon_0}}\right)\cosh(px)\sin(hy-\omega t) \\ &= \gamma_{\rm rf}^2 E_{\rm rf}\left(1-\beta_{\rm rf}^2\right)\cosh(px)\sin(hy-\omega t), \\ H'_{\sim z} &= \gamma_{\rm rf}^2\beta_{\rm rf}E_{\rm rf}\left(\frac{\mu_0}{\sqrt{\mu_0/\varepsilon_0}}-\frac{1}{c}\right)\cosh(px)\sin(hy-\omega t)=0, \end{aligned} \tag{37}$$

or

$$\begin{aligned} E'_{\sim y} &= E_{\rm rf}\sinh(px)\cos(hy-\omega t), \\ E'_{\sim x} &= E_{\rm rf}\cosh(px)\sin(hy-\omega t), \\ H'_{\sim z} &= 0. \end{aligned} \tag{38}$$

It follows from Eqs. (38) that the EMF$^{\rm rf}$ is purely electric (zero $H'_{\sim}$ field) and nonrelativistic; one can compare Eqs. (38) with Eqs. (11).

The time-dependent components of the EMF$^{\rm rf}$ [Eqs. (38)], can be rewritten, using Eq. (22), as follows:

$$\begin{aligned} hy-\omega t &= \frac{h}{\gamma_{\rm rf}}\gamma_{\rm rf}y-\omega t = h'\gamma_{\rm rf}y-\omega t = h'\left(\gamma_{\rm rf}y-\frac{\omega}{h'}t\right) = h'\left(\gamma_{\rm rf}y-\frac{\omega\gamma_{\rm rf}}{h}t\right) \\ &= h'\gamma_{\rm rf}\left(y-\frac{\omega}{h}t\right) = h'\gamma_{\rm rf}(y-v_{\rm rf}t) = h'\gamma_{\rm rf}(y-\beta_{\rm rf}ct) = h'y', \end{aligned} \tag{39}$$

where

$$y' = \gamma_{\rm rf}(y-\beta_{\rm rf}ct). \tag{40}$$

Substituting Eq. (40) into Eq. (39) and Eq. (39) into Eqs. (38) gives, taking into account Eq. (23),

$$\begin{aligned} E'_{\sim y} &= E_{\mathrm{rf}} \sinh(px)\cos(h'y') = E_{\mathrm{rf}} \sinh(px)\cos(py'), \\ E'_{\sim x} &= E_{\mathrm{rf}} \cosh(px)\sin(h'y') = E_{\mathrm{rf}} \cosh(px)\sin(py'), \\ H'_{\sim z} &= 0. \end{aligned} \tag{41}$$

It follows from Eqs. (41) that the $\mathrm{EMF}^{\mathrm{rf}}$ can be treated also to be purely electrostatic (not time dependent).

2.2.2. External dc electric and magnetic fields. Care should be taken while transforming the $\mathrm{EMF}^{\mathrm{dc}}$ [Eqs. (25)] from the LFR into the υ_{rf} moving with velocity [Eq. (20)] MFR using the given Lorentz relativistic transformations [Eq. (35)]. The "trick" is that the velocity υ_{rf} [Eq. (20)] of the MFR, where the $\mathrm{EMF}^{\mathrm{dc}}$ [Eqs. (25)] is transformed from the LFR, should be directed in exact accordance with the given configuration of the transformed $\mathrm{EMF}^{\mathrm{dc}}$ [Eqs. (25)] in the LFR. This means that both positive-x directed $E_{\perp \mathrm{x}}$ and positive-z directed $H_{\perp z}$ fields [Eqs. (25)] are transformed into the MFR using Eq. (35) as [Ref. 36, p. 171, Eqs. (4-9-3)]:

$$E'_{\perp x} = \gamma_{\mathrm{rf}}\left[E_{\perp x} - c(-\beta_{\mathrm{rf}})\mu_0 H_{\perp z}\right] = \gamma_{\mathrm{rf}}\left(E_{\perp x} + c\beta_{\mathrm{rf}}\mu_0 H_{\perp z}\right), \tag{42a}$$

$$H'_{\perp z} = \gamma_{\mathrm{rf}}\left(H_{\perp z} - \frac{-\beta_{\mathrm{rf}}}{c\mu_0}E_{\perp x}\right) = \gamma_{\mathrm{rf}}\left(H_{\perp z} + \frac{\beta_{\mathrm{rf}}}{c\mu_0}E_{\perp x}\right), \tag{42b}$$

where the negative-y directed velocity of the MFR, $-\beta_{\mathrm{rf}} = -\beta_{\mathrm{dc}}$ [Eq. (27)], is determined by both positive-x directed $E_{\perp x}$ and positive-z directed $H_{\perp z}$ fields.

Substituting negative-x directed E_0 and positive-z directed H_0 fields [Eqs. (25)] into [Eqs. (42)] gives

$$\begin{aligned} E'_{\perp x} &= \gamma_{\mathrm{rf}}\left(-E_0 + c\beta_{\mathrm{rf}}\mu_0 H_0\right) = -\gamma_{\mathrm{rf}}\left(E_0 - c\beta_{\mathrm{rf}}\mu_0 H_0\right) \\ &= -\gamma_{\mathrm{rf}}\left(E_0 - c\beta_{\mathrm{rf}}\frac{E_0}{c\beta_{\mathrm{dc}}}\right) = -\gamma_{\mathrm{rf}}E_0\left(1 - \frac{\beta_{\mathrm{rf}}}{\beta_{\mathrm{dc}}}\right), \\ H'_{\perp z} &= \gamma_{\mathrm{rf}}\left[H_0 + \frac{\beta_{\mathrm{rf}}}{c\mu_0}(-E_0)\right] = \gamma_{\mathrm{rf}}\left(H_0 - \frac{\beta_{\mathrm{rf}}}{c\mu_0}E_0\right) \\ &= \gamma_{\mathrm{rf}}\left(H_0 - \frac{\beta_{\mathrm{rf}}}{c\mu_0}c\beta_{\mathrm{dc}}\mu_0 H_0\right) = \gamma_{\mathrm{rf}}H_0\left(1 - \beta_{\mathrm{rf}}\beta_{\mathrm{dc}}\right). \end{aligned} \tag{43}$$

Taking into account that

$$\begin{aligned} \gamma_{\mathrm{rf}}\left(1 - \beta_{\mathrm{rf}}\beta_{\mathrm{dc}}\right) &= \gamma_{\mathrm{rf}}\left(1 - \frac{\beta_{\mathrm{rf}}^2\beta_{\mathrm{dc}}}{\beta_{\mathrm{rf}}}\right) = \gamma_{\mathrm{rf}}\frac{\beta_{\mathrm{dc}}}{\beta_{\mathrm{rf}}}\left(\frac{\beta_{\mathrm{rf}}}{\beta_{\mathrm{dc}}} - \beta_{\mathrm{rf}}^2\right) \\ &= \gamma_{\mathrm{rf}}\frac{\beta_{\mathrm{dc}}}{\beta_{\mathrm{rf}}}\left(1 - \beta_{\mathrm{rf}}^2 - 1 + \frac{\beta_{\mathrm{rf}}}{\beta_{\mathrm{dc}}}\right) = \gamma_{\mathrm{rf}}\frac{\beta_{\mathrm{dc}}}{\beta_{\mathrm{rf}}}\frac{\gamma_{\mathrm{rf}}^2}{\gamma_{\mathrm{rf}}^2}\left(\frac{1}{\gamma_{\mathrm{rf}}^2} - 1 + \frac{\beta_{\mathrm{rf}}}{\beta_{\mathrm{dc}}}\right) \\ &= \frac{\beta_{\mathrm{dc}}}{\gamma_{\mathrm{rf}}\beta_{\mathrm{rf}}}\left[\frac{\gamma_{\mathrm{rf}}^2}{\gamma_{\mathrm{rf}}^2} - \gamma_{\mathrm{rf}}^2\left(1 - \frac{\beta_{\mathrm{rf}}}{\beta_{\mathrm{dc}}}\right)\right] = \frac{\beta_{\mathrm{dc}}}{\gamma_{\mathrm{rf}}\beta_{\mathrm{rf}}}\left[1 - \left(1 - \frac{\beta_{\mathrm{rf}}}{\beta_{\mathrm{dc}}}\right)\gamma_{\mathrm{rf}}^2\right] \end{aligned} \tag{44}$$

and substituting Eq. (32) into Eq. (44) and both Eqs. (32) and (44) into Eq. (43) gives the $\mathrm{EMF}^{\mathrm{dc}}$ written as [Ref. 22, p. 116, Eq. (2.2)]

$$E'_{\perp x} = -\alpha\gamma_{\mathrm{rf}}E_0, \tag{45a}$$

$$H'_{\perp z} = H_0\frac{\beta_{\mathrm{dc}}}{\gamma_{\mathrm{rf}}\beta_{\mathrm{rf}}}\left(1-\alpha\gamma_{\mathrm{rf}}^2\right) = \frac{E_0}{c\beta_{\mathrm{dc}}\mu_0}\frac{\beta_{\mathrm{dc}}}{\gamma_{\mathrm{rf}}\beta_{\mathrm{rf}}}\left(1-\alpha\gamma_{\mathrm{rf}}^2\right) = \frac{E_0}{\sqrt{\mu_0/\varepsilon_0}}\frac{1}{\gamma_{\mathrm{rf}}\beta_{\mathrm{rf}}}\left(1-\alpha\gamma_{\mathrm{rf}}^2\right). \tag{45b}$$

Under synchronous conditions (31), $\alpha = 0$, the $\mathrm{EMF}^{\mathrm{dc}}$ (45) can be written as [Ref. 14, p. 285, Eq. (4)]

$$E'_{\perp x} = 0, \tag{46a}$$

$$H'_{\perp z} = \frac{H_0}{\gamma_{\mathrm{rf}}} = \gamma_{\mathrm{rf}}H_0\left(1-\beta_{\mathrm{rf}}^2\right). \tag{46b}$$

2.2.3. Total electric and magnetic fields. The $\mathrm{EMF}^{\mathrm{rf/dc}}$ affecting electron motion in the planar magnetron (Fig. 3) is the superposition of the $\mathrm{EMF}^{\mathrm{rf}}$ (41) and the $\mathrm{EMF}^{\mathrm{dc}}$ (45):

$$E'_y = E'_{\sim_y} = E_{\mathrm{rf}}\sinh(px)\cos(py'), \tag{47a}$$

$$E'_x = E'_{\perp x} + E'_{\sim_x} = -\alpha\gamma_{\mathrm{rf}}E_0 + E_{\mathrm{rf}}\cosh(px)\sin(py'), \tag{47b}$$

$$H'_z = H'_{\perp z} = \frac{E_0}{\sqrt{\mu_0/\varepsilon_0}}\frac{1}{\gamma_{\mathrm{rf}}\beta_{\mathrm{rf}}}\left(1-\alpha\gamma_{\mathrm{rf}}^2\right). \tag{47c}$$

Under synchronous conditions (31), $\alpha = 0$, both the E'_y (47a) and E'_x (47b) electric field components of the $\mathrm{EMF}^{\mathrm{rf/dc}}$ (47) are determined only by the $E'_\sim$ field (41).

The E'_y (47a) and E'_x (47b) field distributions are shown in Figs. 4 and 5 at the AK voltage $V_0 = 350$ kV and, respectively, two magnetic flux densities, $B_0 = \mu_0 H_0 = 0.72$ T, which is very popular in analyzing results of 2D PIC simulations of the A6 magnetron operating in the π mode (see references in Ref. 9), and $B_0 = 1.01$ T, when the drift velocity v_{dc} (27) in the LFR equals the phase velocity v_{rf} (20), resulting in synchronous condition of the magnetron operation (31), $\alpha = 0$.

To plot both E'_y and E'_x distributions (Figs. 4 and 5), the $E_\sim$ field amplitude E_1 (7) is taken to be equal to the $E_\perp$ field amplitude E_0 (8a), which is the "zero-order-magnitude" approximation

$$E_1 = 10^0 \cdot E_0, \tag{48}$$

the ordinate is naturally bounded by the AK spacing d (51),

$$0 \le px \le pd, \tag{49}$$

and the abscissa is naturally determined by one wavelength, 2π, of the $\mathrm{EMF}^{\mathrm{rf}}$ (41):

$$-\pi \le py' \le \pi. \tag{50}$$

All geometrical parameters used to plot both E'_y and E'_x distributions (Figs. 4 and 5) correspond to the 2D geometry of the A6 magnetron ($r_c = 1.58$ cm, $r_a = 2.11$ cm) operating in the π mode with frequency $f = 1.95$ GHz. Transformation from the cylindrical geometry of a multicavity magnetron (determined by the cathode and the anode radii, r_c and r_a) to its planar model (Fig. 3) (determined by the AK spacing d only) and length of one spatial

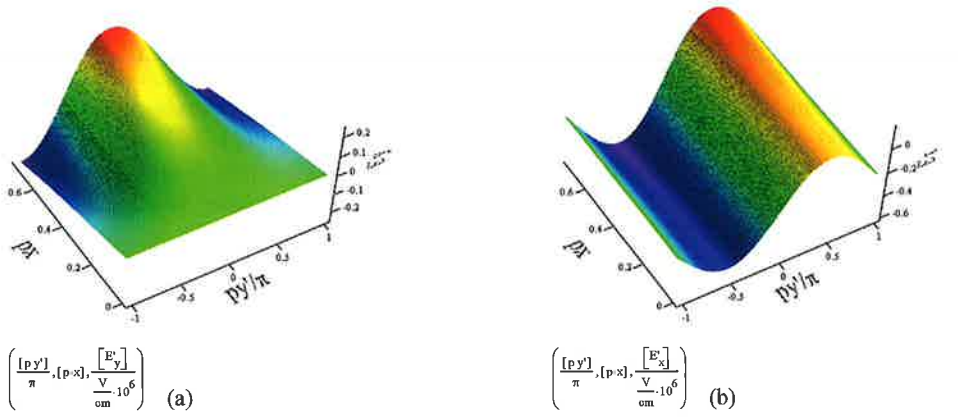

Fig. 4. Distribution of (a) E'_y (47a) and (b) E'_x (47b) fields at $\alpha = 0.282$, $B_0 = 0.72$ T, and $V_0 = 350$ kV.

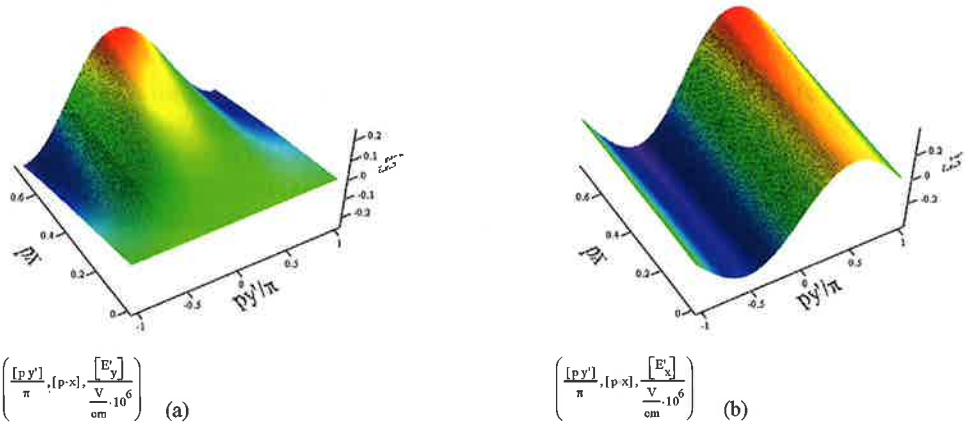

Fig. 5. Distribution of (a) E'_y (47a) and (b) E'_x (47b) fields at $\alpha \sim 0$, $B_0 = 1.01$ T, and $V_0 = 350$ kV.

period D is performed as follows [Ref. 6, p. 273, Eq. (7.7); Ref. 26, p. 987, Eq. (2); and Ref. 13, p. 363], which is the "planar-geometry-magnetron" approximation:

$$d = \frac{r_a^2 - r_c^2}{2r_a}, \tag{51}$$

$$D = 2\pi r_e / N, \tag{52}$$

where N is the total number of cavities of a multicavity magnetron and r_e is the effective radius at which the phase velocity of the traveling rf wave υ_{rf} (20) is compared with the drift velocity of electrons υ_{dc} (27) specifying in this way the detuning coefficient α (32). In accordance with Ref. 19 [p. 540, Eq. (18)] and Ref. 14 [p. 287, Eq. (7)], the effective radius r_e is defined as the middle radius r_m of the AK spacing:

$$r_c < r_e \equiv r_m = \frac{r_a + r_c}{2} < r_a, \tag{53}$$

which corresponds to the case when the electron sheath boundary is located in the geometrical center between the cathode and the anode.

Comparing Fig. 4 with Fig. 5 shows that the E'_y field distribution (47a) is the same in both cases. This is because the E'_y (47a) field does not depend on the detuning coefficient α, which means that it does not depend on the external dc magnetic field H_0. However, the E'_x field distribution (47a) at the lower magnetic field H_0 and the positive detuning coefficient α (Fig. 4b) is lower than the E'_x field distribution (47a) at the higher magnetic field H_0 and $\alpha = 0$ (Fig. 5b). This is because the E'_x (47a) field does depend on the detuning coefficient α and, hence, on the external dc magnetic field H_0.

Notice that within the space bounded by conditions (49) and (50) (Figs. 4 and 5), there is only one of n periodically repeated distributions of the $\mathrm{EMF}^{\mathrm{rf/dc}}$ (47). Thus, the number n corresponds to the total number of wavelengths of the traveling rf wave that fits within the azimuthal length of the cylindrical magnetron; it equals also one half, $N/2$, of the total number of cavities for the π-mode electric field distribution:

$$n = N/2. \tag{54}$$

Thus, there is only one single magnetron spoke, $n = 1$, in the space bounded by conditions (49) and (50).

2.2.4. About the effective radius r_e determining length of one spatial period D, longitudinal wave number h, phase velocity of the traveling rf wave v_{rf}, and, finally, detuning coefficient α. The effective radius r_e can be also chosen to be either the anode radius r_a (Ref. 34, p. 1350) when the synchronous condition (31) and (32) "is evaluated for the case of the electron sheath extending to the anode; the result is termed the Buneman–Hartree threshold" [Ref. 18, p. 229, Eq. (6.30)] and corresponds to a minimum magnetic field at which, at a given AK voltage, the π mode of magnetron oscillations can occur:

$$r_e \equiv r_a, \tag{55}$$

or with the cathode radius r_c as the ultimate case corresponding to the zero-thickness electron sheath, $x_b = 0$, the result corresponds to a maximum magnetic field at which, at a given AK voltage, the π mode of magnetron oscillations can occur:

$$r_e \equiv r_c. \tag{56}$$

One can suppose also that there is a dependence of the r_e radius on the input parameters of a magnetron operation, i.e., on the external dc electric E_0 and magnetic H_0 fields, which corresponds to the appropriate dependence of the electron sheath thickness or the "boundary line" (33). In this case the effective radius r_e is determined as

$$r_e \equiv r_b = r_c + x_b = r_c + 2r_L(E_0, H_0). \tag{57}$$

It follows from Eq. (57) that in this case the r_b radius varies, with changing either or both the magnetic field H_0 and the AK voltage V_0, within the limits determined by its maximum (55) and minimum (56) values:

$$r_a \geq r_b(H_0, V_0) \geq r_c. \tag{58}$$

Thus the effective radius r_e is defined as the radial position in a cylindrical magnetron (see Fig. 12 later in the paper) or the x coordinate in a planar magnetron (Fig. 3), where the drift velocity of an electron v_{dc} (27) is compared with the phase velocity of the traveling rf wave v_{rf} (20) specifying in this way the detuning coefficient α (32). From that radius r_e, which is

determined also as the "boundary line" x_b (33) of the electron sheath, an electron starts to drift to the anode. There are then four different I_a^{cal} (91) that are defined differently assuming that, at the given AK voltage V_0, either the effective radius r_e does not vary with the magnetic field H_0 variation and (1) in accordance with expression (55), r_e equals the anode radius r_a (Ref. 34, p.1350), when the Larmor radius is maximum, $2r_L = r_a - r_c$, at the minimum magnetic field, allowing the π mode of magnetron oscillations to occur, or (2) in accordance with relation (56), the r_e equals the cathode radius r_c when the Larmor radius is minimum, $r_L \sim 0$, at maximum magnetic field allowing the π mode of magnetron oscillations to occur, or (3) in accordance with expression (53), the r_e equals the middle radius r_m of the AK spacing [Ref. 19, p. 540, Eq. (18); Ref. 14, p. 287, Eq. (7)] at intermediate Larmor radii and magnetic fields allowing the π mode of magnetron oscillations to occur, or the effective radius r_e does vary with the magnetic field H_0 variation, and (4) in accordance with expression (57), the r_e varies with the magnetic field variation within the limits determined by expression (58); this assumption models the effect of the magnetic field H_0 change on the electron sheath thickness and, respectively, on I_a^{cal} (91) dependence on magnetic field H_0.

Whereas the E'_y (47a) and E'_x (47b) field distributions shown in Figs. 4 and 5 are obtained using the effective radius r_e defined as the middle radius r_m (53), all four different definitions of the effective radius r_e [(53), (55)–(57)] will be used to calculate analytically the anode current of the relativistic A6 magnetron operating in the π mode with a frequency of 1.95 GHz.

2.2.5. Electron motion in the moving frame of reference. In the absence of EMF^{rf} (41), when the E_1 amplitude (7) is zero, an electron moves in the EMF^{dc} (45) only, along a trajectory, which is the superposition of (i) the electron drift along the cathode with the drift velocity υ'_{dc} defined as

$$\upsilon'_{\text{dc}} = -\frac{1}{\mu_0}\frac{E'_{\perp x}}{H'_{\perp z}} = -\frac{\alpha\gamma_{\text{rf}}E_0}{\mu_0 H_0 \dfrac{\beta_{\text{dc}}}{\gamma_{\text{rf}}\beta_{\text{rf}}}\left(1-\alpha\gamma_{\text{rf}}^2\right)} = \frac{E_0}{\mu_0 H_0}\frac{\gamma_{\text{rf}}^2\beta_{\text{rf}}}{\beta_{\text{dc}}}\frac{\alpha}{1-\alpha\gamma_{\text{rf}}^2}$$

$$= c\gamma_{\text{rf}}^2\beta_{\text{rf}}\frac{\alpha}{1-\alpha\gamma_{\text{rf}}^2} = \gamma_{\text{rf}}^2\upsilon_{\text{rf}}\frac{\alpha}{1-\alpha\gamma_{\text{rf}}^2}, \tag{59}$$

and (ii) the electron gyration in the plane perpendicular to the $H'_{\perp z}$ field (45b), with the cyclotron frequency ω'_c [Ref. 17, p. 53, Eq. (21.3); Ref. 14, p. 285; Ref. 36, p. 172, Eq. (4-9-7)] and the Larmor radius r'_L [Ref. 17, p. 53, Eq. (21.6); Ref. 36, p. 172, Eq. (4-9-8)]:

$$\omega'_c = \frac{|q_e|}{m'_e}\mu_0 H'_{\perp z} = \frac{|q_e|}{m_e\gamma_{\text{rf}}}\mu_0 H_0\frac{\beta_{\text{dc}}}{\gamma_{\text{rf}}\beta_{\text{rf}}}\left(1-\alpha\gamma_{\text{rf}}^2\right), \tag{60}$$

$$r'_L = \frac{|\upsilon'_\perp|}{\omega'_c} = \frac{|\upsilon'_0 + \upsilon'_{\text{dc}} - \upsilon_{\text{rf}}|m_e\gamma_{\text{rf}}}{|q_e|\mu_0 H_0\dfrac{\beta_{\text{dc}}}{\gamma_{\text{rf}}\beta_{\text{rf}}}\left(1-\alpha\gamma_{\text{rf}}^2\right)} = \frac{|-\upsilon_{\text{rf}} + \upsilon'_{\text{dc}}|m_e}{|q_e|\mu_0 H_0}\frac{\gamma_{\text{rf}}^2\beta_{\text{rf}}}{\beta_{\text{dc}}\left(1-\alpha\gamma_{\text{rf}}^2\right)}$$

$$= \frac{|-\upsilon_{\text{rf}} + \upsilon'_{\text{dc}}|m_e}{|q_e|\dfrac{E_0}{c\beta_{\text{dc}}}}\frac{\gamma_{\text{rf}}^2\beta_{\text{rf}}}{\beta_{\text{dc}}\left(1-\alpha\gamma_{\text{rf}}^2\right)} = \frac{|-\upsilon_{\text{rf}} + \upsilon'_{\text{dc}}|c\gamma_{\text{rf}}^2\beta_{\text{rf}}}{1-\alpha\gamma_{\text{rf}}^2}\frac{m_e}{q_e E_0}, \tag{61}$$

where the "effective" velocity $\upsilon'_\perp$ is the superposition of the drift velocity υ'_{dc} (59) in the MFR, the intrinsic velocity of the MFR υ_{rf} (27), and the "initial" velocity $\upsilon'_0 = 0$, with

which the cathode emits the electron:

$$\upsilon'_{\perp} = \upsilon'_0 + \upsilon'_{\rm dc} - \upsilon_{\rm rf} = -\upsilon_{\rm rf} + \upsilon'_{\rm dc}. \tag{62}$$

Under the synchronous conditions (31), $\alpha = 0$, an electron does not drift anywhere because the $E'_{\perp x}$ is zero (46a) and, hence, the drift velocity $\upsilon'_{\rm dc}$ (59) is also zero. Electrons only gyrate near the cathode in the plane perpendicular to the H'_z field with the cyclotron frequency ω'_c [Ref. 14, p. 285, Eq. (4)] and the Larmor radius [Ref. 22, p. 117, Eq. (2.4)] defined as

$$\omega'_c = \frac{|q_e|\,\mu_0 H_0}{m_e \gamma_{\rm rf}^2} = \frac{\omega_c}{\gamma_{\rm rf}^2}. \tag{63}$$

$$r'_L = \upsilon_{\rm rf} c \gamma_{\rm rf}^2 \beta_{\rm rf} \frac{m_e}{q_e E_0} = c^2 \beta_{\rm rf}^2 \gamma_{\rm rf}^2 \frac{m_e}{|q_e|\,E_0} = c^2 \beta_{\rm dc}^2 \gamma_{\rm rf}^2 \frac{m_e}{|q_e|\,E_0}$$

$$= c^2 \frac{\gamma_{\rm rf}^2 - 1}{\gamma_{\rm rf}^2} \gamma_{\rm rf}^2 \frac{m_e}{q_e E_0} = \frac{m_e c^2}{q_e E_0} \left(\gamma_{\rm rf}^2 - 1\right) = r_L \gamma_{\rm rf}^2. \tag{64}$$

The dependence of the r'_L (64) on $\gamma_{\rm rf}^2$ results in the fact that the Larmor radius along the cathode, i.e., in the direction to which the MFR moves, $r'_{L\parallel}$, is by a factor $\gamma_{\rm rf}^2$ larger than the Larmor radius in the direction across the cathode, $r'_{L\perp}$. Positions of the "feeding line" x'_f and the "boundary line" x'_b in the MFR are determined by one and two Larmor radii, respectively, in the direction across the cathode, $r'_{L\perp}$:

$$x'_f = r'_{L\perp} = r_L, \tag{65}$$

$$x'_b = 2r'_{L\perp} = 2r_L. \tag{66}$$

When the amplitude E_1 (12) is sufficiently not zero, an electron moves in the EMF$^{\rm rf/dc}$ (47) along a trajectory, which is a superposition of (i) the electron drift in the crossed E'_x (26b) and H'_z (26c) fields, i.e., the $E'_x \mathrm{x} H'_z$ drift pushing electrons in either the positive or negative $\pm y$ (along the cathode) direction, (ii) the electron drift in the crossed E'_y (26a) and H'_z (26c) fields, i.e., the $E'_y \times H'_z$ drift pushing electrons in either the positive or negative $\pm x$ (crosswise to the cathode) direction, and (iii) the electron cyclotron gyration (63), (64) in the plane perpendicular to the H'_z (26c) field.

2.3. Electron drift in the moving frame of reference

2.3.1. Electron drifts. It follows from Eqs. (47) that the H'_z (47c) field is uniform and always directed along the z axis, whereas both E'_y (47a) [Fig. 4(a)] and E'_x (47b) [Fig. 4(b)] fields are nonuniform and spatially varying due to their dependencies on appropriate trigonometric and hyperbolic functions. To illustrate those variations, both E'_y [(47a); Fig. 4(a)] and E'_x [(47b); Fig. 4(b)] field distributions are plotted in Figs. 6 and 7 at a number of fixed distances px between the cathode and the anode at the AK voltage $V_0 = 350$ kV and, respectively, two magnetic flux densities, $B_0 = 0.72$ T, $\alpha = 0.282$, and $B_0 = 1.01$ T, $\alpha \sim 0$. One can compare these distributions with those plotted in Figs. 4 and 5, respectively, and find that there can be defined three characteristic lines dividing the space bounded by conditions (49) and (50) into a number of separate regions with different directions of appropriate electric fields, E'_y and E'_x, within them.

The first two characteristic lines define three separate regions with different directions of the E'_y field [Figs. 6(a) and 7(a)]. Along these two characteristic lines (that can be called the

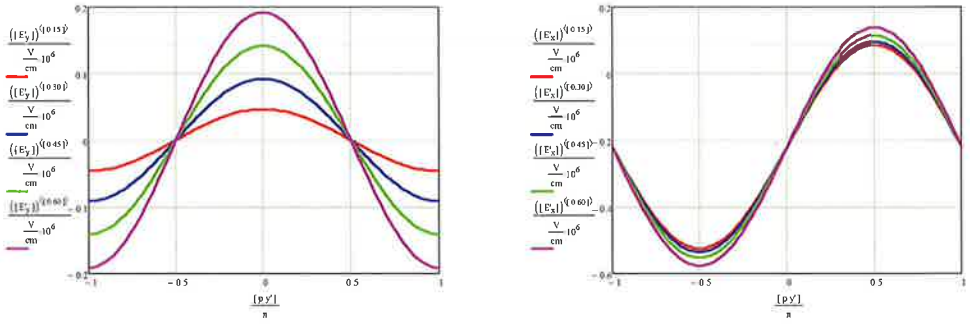

(a) (b)

Fig. 6. Distribution of E'_y (47a) (a) and E'_x (47b) (b) fields at $px = 0.15$, 0.30, 0.45, and 0.60 ($\alpha = 0.282$, $B_0 = 0.72$ T, $V_0 = 350$ kV).

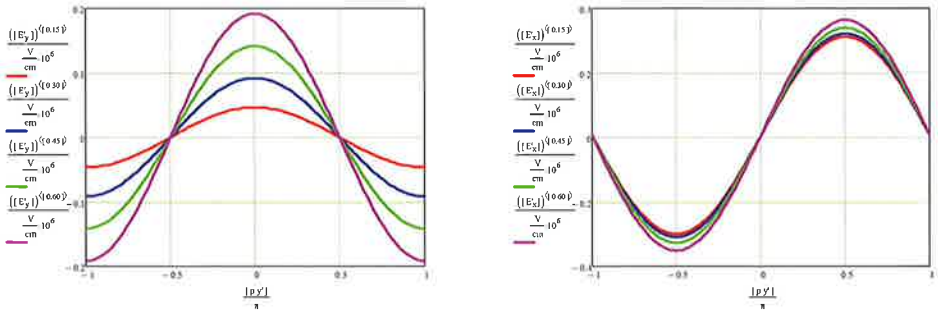

(a) (b)

Fig. 7. Distribution of E'_y (47a) (a) and E'_x (47b) (b) fields at $px = 0.15$, 0.30, 0.45, and 0.60 ($\alpha \sim 0$, $B_0 = 1.01$ T, $V_0 = 350$ kV).

"lines of asynchronism") the E'_y field is zero [Figs. 6(a) and 7(a)]. It follows from Eq. (47a) that to satisfy this requirement, i.e.,

$$E'_y = E_{\text{rf}} \sinh(px) \cos(py') = 0, \tag{67}$$

the following condition should be met:

$$py' = \text{acos}(0). \tag{68}$$

Equation (68) has two obvious solutions, which are [Fig. 6(a)]

$$py' = \pm\pi/2. \tag{69}$$

The crossed *positive-y*-directed E'_{+y} field and *positive-z*-directed H'_{+z} field produce an electron drift in the *positive-x* direction, whereas the crossed *negative-y*-directed E'_{-y} field and *positive-z*-directed H'_{+z} field produce the electron drift in the *negative-x* direction. Thus these two "lines of asynchronism" (69) also divide all electrons drifting crosswise to the cathode into electrons drifting toward the anode and electrons drifting toward the cathode, i.e., into electrons located in a favorable or in an unfavorable phase of the E'_y (47) field. The central region where electrons are in the favorable phase of the E'_y field and where they

drift in the crossed $E'_{+y}xH'_{+z}$ fields from the cathode toward the anode is bounded by the following condition:

$$-\pi/2 \le py' \le \pi/2, \tag{70}$$

which gives total length of the emitting area in the y'-direction L'_y in the MFR:

$$pL'_y = \pi. \tag{71}$$

The two adjacent regions where electrons are in the nonfavorable phase of the E'_y field and where they drift in the crossed $E'_{-y} \times H'_{+z}$ fields back to the cathode are bounded by the following condition:

$$-\pi/2 \ge py' \ge \pi/2. \tag{72}$$

It is important to note at this point that the electron drift caused by the crossed $E'_y \times H'_z$ fields (47) is determined only by the $E'_{\sim y}$ (41) and the $H'_{\perp z}$ fields (45b), whereas the $E'_{\perp x}$ field does not affect this electron drift. The velocity of the electron drift crosswise to the cathode is determined as follows:

$$\upsilon'_x = -\frac{1}{\mu_0}\frac{E'_y}{H'_z} = -\frac{1}{\mu_0}\frac{E_{\mathrm{rf}}\sinh(px)\cos(py')}{\frac{E_0}{\sqrt{\mu_0/\varepsilon_0}}\frac{1}{\gamma_{\mathrm{rf}}\beta_{\mathrm{rf}}}\left(1-\alpha\gamma_{\mathrm{rf}}^2\right)} = -\frac{\gamma_{\mathrm{rf}}\beta_{\mathrm{rf}}}{\sqrt{\mu_0\varepsilon_0}}\frac{E_{\mathrm{rf}}}{E_0}\frac{\sinh(px)\cos(py')}{1-\alpha\gamma_{\mathrm{rf}}^2}$$

$$= -\gamma_{\mathrm{rf}}c\beta_{\mathrm{rf}}\frac{E_{\mathrm{rf}}}{E_0\left(1-\alpha\gamma_{\mathrm{rf}}^2\right)}\sinh(px)\cos(py') = -\gamma_{\mathrm{rf}}\upsilon_{\mathrm{rf}}\frac{E_{\mathrm{rf}}}{E_0\left(1-\alpha\gamma_{\mathrm{rf}}^2\right)}\sinh(px)\cos(py'). \tag{73}$$

The third characteristic line defines two separate regions with different directions of the E'_x [Figs. 6(b) and 7(b)] field. At this characteristic line (that can be called the "line of synchronism"), the E'_x field is zero. It follows from Eq. (47b) that that to satisfy this requirement, i.e.,

$$E'_x = -\alpha\gamma_{\mathrm{rf}}E_0 + E_{\mathrm{rf}}\cosh(px)\sin(py') = 0, \tag{74}$$

the following condition should be met:

$$py' = \operatorname{asin}\left(\frac{\alpha\gamma_{\mathrm{rf}}E_0}{E_{\mathrm{rf}}\cosh(px)}\right). \tag{75}$$

Under synchronous conditions (31), Eq. (75) has the only obvious solution, which is

$$py' = 0. \tag{76}$$

The crossed *negative-x*-directed E'_{-x} field and *positive-z*-directed H'_{+z} field produce the electron drift in the *positive-y* direction, whereas the crossed *positive-x*-directed E'_{+x} field and *positive-z*-directed H'_{+z} field produce the electron drift in the *negative-y* direction. Thus, the "line of synchronism" (75) or (76) also divides all electrons drifting along the cathode into electrons drifting cocurrent with the traveling rf wave (in the *positive*-y direction) and electrons drifting countercurrent with the traveling rf wave (in the *negative-y* direction). The left-side region where electrons are forced by the crossed $E'_{-x}xH'_{+z}$ fields to drift in one direction with the traveling rf wave is bounded [under synchronous conditions (31)] by the following condition:

$$-\pi/2 \le py' \le 0, \tag{77}$$

and the right-side region where electrons are forced by the crossed $E'_{+x} \times H'_{+z}$ fields to drift toward the traveling rf wave is bounded [under synchronous conditions (31)] by the following condition:

$$0 \le py' \le \pi/2. \tag{78}$$

The electron drift caused by the crossed $E'_x \mathrm{x} H'_z$ fields (47) is determined by both $E'_{\sim x}$ (41) and $E'_{\perp x}$ fields and the $H'_{\perp z}$ field (45b). However, under synchronous conditions (31), only the $E'_{\sim x}$ (41) and the $H'_{\perp z}$ (45b) fields affect this drift, whereas the $E'_{\perp x}$ field does not affect it. The velocity of the electron drift along the cathode is determined as follows:

$$\begin{aligned} \upsilon'_y &= -\frac{1}{\mu_0}\frac{E'_x}{H'_z} = -\frac{1}{\mu_0}\frac{-\alpha\gamma_{\mathrm{rf}}E_0 + E_{\mathrm{rf}}\cosh(px)\sin(py')}{\dfrac{E_0}{\sqrt{\mu_0/\varepsilon_0}}\dfrac{1}{\gamma_{\mathrm{rf}}\beta_{\mathrm{rf}}}\left(1-\alpha\gamma_{\mathrm{rf}}^2\right)} \\ &= \frac{\alpha\gamma_{\mathrm{rf}}E_0 - E_{\mathrm{rf}}\cosh(px)\sin(py')}{\sqrt{\mu_0\varepsilon_0}\dfrac{E_0}{\gamma_{\mathrm{rf}}\beta_{\mathrm{rf}}}\left(1-\alpha\gamma_{\mathrm{rf}}^2\right)} = c\gamma_{\mathrm{rf}}\beta_{\mathrm{rf}}\frac{\alpha\gamma_{\mathrm{rf}}E_0 - E_{\mathrm{rf}}\cosh(px)\sin(py')}{E_0\left(1-\alpha\gamma_{\mathrm{rf}}^2\right)} \\ &= \gamma_{\mathrm{rf}}\upsilon_{\mathrm{rf}}\frac{\alpha\gamma_{\mathrm{rf}}E_0 - E_{\mathrm{rf}}\cosh(px)\sin(py')}{E_0\left(1-\alpha\gamma_{\mathrm{rf}}^2\right)}. \end{aligned} \tag{79}$$

Thus, the total electron drift between the cathode and the anode is a superposition of (i) the cathode-to-anode drift υ'_x (73) of those electrons whose initial position is in the favorable phase of the traveling rf wave (70) and (ii) the side-to-center inwardly directed drift υ'_y (79) of these electrons. The unique combination of two different kinds of drifts with the drift velocities υ'_x (73) and υ'_e (79) as well as the cyclotron gyration (63) and (64) of electrons forms the well-known geometry of a magnetron spoke typically observed in PIC simulations of a magnetron operation.

Both drift velocities υ'_x (73) and υ'_y (79) are determining by taking into account only the external dc $\mathrm{EMF}^{\mathrm{dc}}$ (45) and the induced rf $\mathrm{EMF}^{\mathrm{rf}}$ (41) and by ignoring additional electric and magnetic fields produced by the electron space charge of the drifting within the formed magnetron spoke electrons. Thus the electron drift between the cathode and the anode with the drift velocities υ'_x (73) and υ'_y (79) is considered to be not perturbed by this space charge, which is the "zero-space-charge" approximation.

2.3.2. Electron trajectories. In the case when the radius of the cyclotron gyration r_L (30) of drifting electrons is sufficiently less than the distance between the top boundary of the electron sheath and the anode, i.e., when

$$r_L \ll d_e - x_b, \tag{80}$$

the electron gyration can be ignored and an electron movement within the formed magnetron spoke can be approximated only by the pair of transverse one to another drift of an electron guiding center (egcon), υ'_x (73) and υ'_y (79), determined by an appropriate pair of the crossed $E'_x \times H'_z$ and $E'_y \times H'_z$ (47) fields (the "guiding-centers-motion" approximation).

The egcon trajectories coincide with equipotential lines picturing the scalar φ' potential distribution between the cathode and the anode. Taking into account that the electric field is determined, in the general case, as [Ref. 17, p. 50, Eq. (19.1)]

$$E = -\nabla\varphi, \tag{81}$$

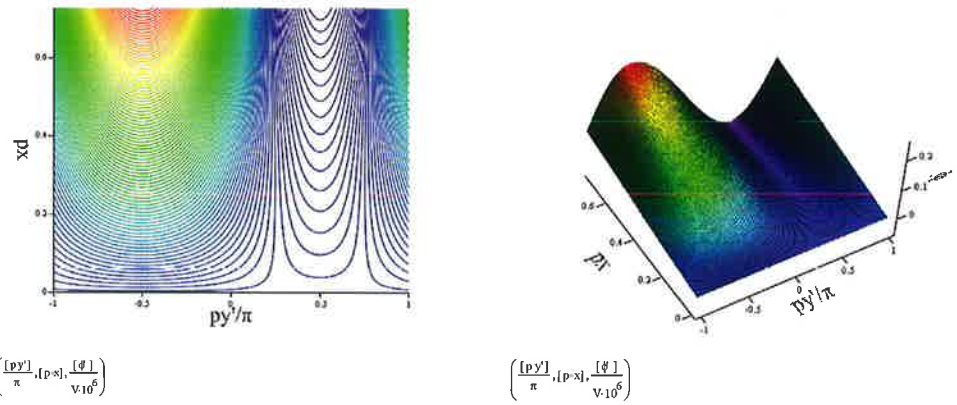

Fig. 8. Scalar φ' potential (82) distribution in the MFR at $\alpha = 0.282$, $B_0 = 0.72$ T, and $V_0 = 350$ kV.

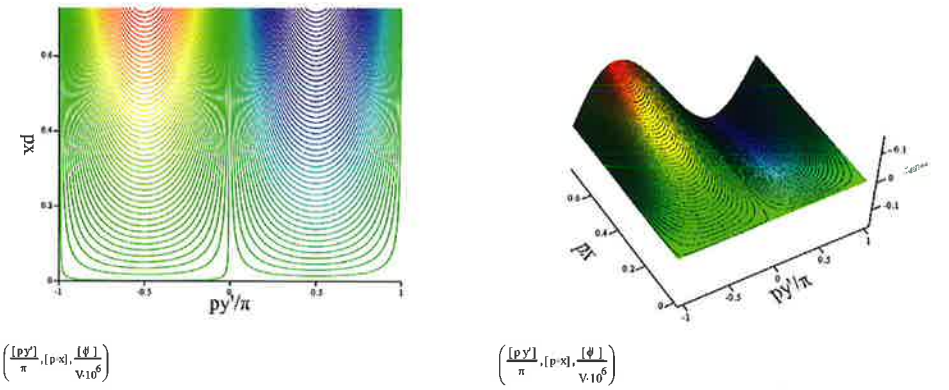

Fig. 9. Scalar φ' potential (82) distribution in the MFR at $\alpha \sim 0$, $B_0 = 1.01$ T, and $V_0 = 350$ kV.

one can find the potential distribution φ' by integrating, for example, the E'_x (47) field of the $\text{EMF}^{\text{rf/dc}}$ [Ref. 22, p. 116–117, Eqs. (2.1) and (2.6)]:

$$\varphi' = \alpha\gamma_{\text{rf}} E_0 x - \frac{E_1}{p}\sinh(px)\sin(py'). \tag{82}$$

Distributions of the φ' potential (82) are shown in Figs. 8 and 9 at the AK voltage $V_0 = 350$ kV and, respectively, two magnetic field flux densities $B_0 = 0.72$ T when $\alpha = 0.282$ and 1.01 T when $\alpha \sim 0$. These distributions correspond to the distributions of the electric field components of the $\text{EMF}^{\text{rf/dc}}$ shown in Figs. 4 and 5, respectively, and the "zero-space-charge" approximation, when the total space charge of the drifting egcons is ignored.

The trajectories of egcons determined by the appropriate equal-potential lines (Figs. 8 and 9) are shown in Figs. 10 and 11, respectively. Notice that despite the fact that the effective radius r_e (53) used to plot distributions in Figs. 4–9 is defined in the center of the AK spacing at equal distances between the cathode and the anode [Ref. 19, p. 540, Eq. (18); Ref. 14, p. 287, Eq. (7)], the starting position of egcons drifting toward the anode or the "feeding line" for the anode current in the MFR is determined in Figs. 10 and 11 as the Larmor radius in the direction across the cathode (65), as was originally done in

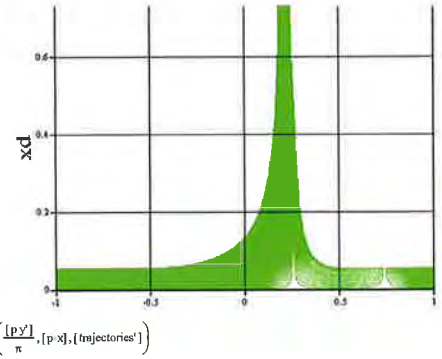

Fig. 10. Single magnetron spoke of the "classical" A6 relativistic magnetron ($\alpha = 0.282$, $B_0 = 0.72$ T, $V_0 = 350$ kV) plotted using the potential distribution φ' (82).

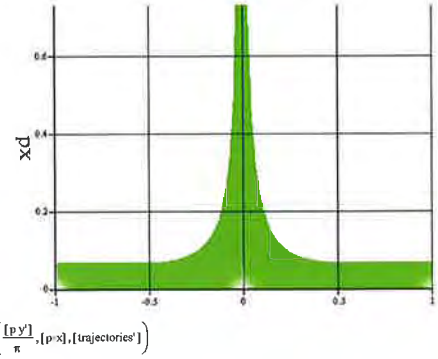

Fig. 11. Single magnetron spoke of the "classical" A6 relativistic magnetron ($\alpha \sim 0$, $B_0 = 1.01$ T, $V_0 = 350$ kV) plotted using the potential distribution φ' (82).

Ref. 21, p. 310, Fig. 1; Ref. 22, p. 119, Fig. 2; Ref. 14, p. 133, Fig. 2.1.3; and Ref. 23, p. 57, Fig. 2.12.

The trajectories of the drifting egcons (Figs. 10 and 11) are obtained using the same "zero-space-charge" approximation.

2.3.3. Magnetron spoke current. A single magnetron spoke current in the MFR I'_s is determined, within the space bounded by conditions (49) and (50), as a product of (i) the crosswise to the cathode velocity v'_x of egcons drifting from the cathode toward the anode in the crossed $E'_x \times H'_z$ and $E'_y \times H'_z$ fields, (ii) the charge density ρ'_e of electrons gyrating within the electron sheath with thickness x'_b (66), and (iii) the emitting area S'_e from where electrons gyrating near the cathode start drifting toward the anode [Ref. 18, p. 233, Eq. (6.45)]:

$$I'_s = v'_x \rho'_e S'_e. \tag{83}$$

The "volume" ρ'_e charge density of electrons gyrating within the electron sheath with thickness x'_b (66) can be averaged along the x direction (crosswise to the cathode), resulting

in the "surface" σ'_e charge density of these electrons:

$$\sigma'_e = \int_0^{x'_b} \rho'_e(x)dx = \rho'_e \int_0^{x'_b} dx = \rho'_e x'_b, \tag{84}$$

where it is supposed that the "volume" ρ'_e charge density along the x direction is uniform. Substituting Eq. (84) into Eq. (83) gives

$$I'_s = \frac{\upsilon'_x \sigma'_e S'_e}{x'_b} = \frac{\upsilon'_x \sigma'_e S'_e}{2r_L} = \upsilon'_x \sigma'_e \frac{L'_y L'_z}{2r_L} = \upsilon'_x \sigma'_e \frac{L'_y L_z}{2r_L}, \tag{85}$$

where L'_y and $L'_z = L_z$ are the cathode lengths in the y and z directions, respectively.

In the case when the cathode operates in the explosive-emission (or the space-charge-limited-emission) mode, the surface charge density σ'_e of electrons is determined by a condition of the total compensation of the electron space charge by the external dc electric field E_0 at the electron sheath boundary [Ref. 22, p. 118, Eq. (2.8)]:

$$\sigma'_e = \frac{\sigma_e}{\gamma_{\text{rf}}} = \frac{\varepsilon_0 E_0}{\gamma_{\text{rf}}}, \tag{86}$$

where the "surface" σ_e charge density in the LFR increases by factor γ_{rf} relative to the surface charge density in the MFR $\sigma'_e = \sigma_e/\gamma_{\text{rf}}$ [Ref. 36, p. 122, Eq. (3-3-5)].

Substituting Eq. (86) into Eq. (85) gives the magnetron spoke current in the MFR:

$$I'_s = \frac{\varepsilon_0 E_0}{\gamma_{\text{rf}}} \frac{L'_y L_z}{2r_L} \int_{py'=-\pi/2}^{py'=\pi/2} \upsilon'_x(px, py')d(py') \Big|_{px=px'_f=px_f=pr_L}, \tag{87}$$

where the integration limits, from $-\pi/2$ to $\pi/2$, are determined by condition (70), and the integration constant, $px = pr_L$, is determined by position of the "feeding line" x'_f from where egcons start drifting toward the anode. Substituting Eq. (73) into Eq. (87) and taking into account Eq. (71) gives the very simple expression for the magnetron spoke current in the MFR:

$$I'_s = -\varepsilon_0 \frac{E_0}{\gamma_{\text{rf}}} \frac{L'_y L_z}{2r_L} \int_{py'=-\pi/2}^{py'=\pi/2} \gamma_{\text{rf}} \upsilon_{\text{rf}} \frac{E_{\text{rf}}}{E_0\left(1-\alpha\gamma_{\text{rf}}^2\right)} \sinh(pr_L)\cos(py')d(py')$$

$$= -\varepsilon_0 \upsilon_{\text{rf}} \frac{\frac{\pi}{p} L_z}{2r_L} \frac{E_{\text{rf}} \sinh(pr_L)\left[\sin(\pi/2) - \sin(-\pi/2)\right]}{1-\alpha\gamma_{\text{rf}}^2} = \varepsilon_0 \upsilon_{\text{rf}} \frac{2E_{\text{rf}} \sinh(pr_L)}{1-\alpha\gamma_{\text{rf}}^2} \frac{\pi L_z}{p2r_L}. \tag{88}$$

The magnetron spoke current whose flow direction is perpendicular to the direction of the MFR movement in the LFR is determined relative to the magnetron spoke current in the MFR (88) as [Ref. 36, p. 124, Eq. (3-4-1); Ref. 17, p. 11, Eqs. (4–5) and (4–6)]

$$I_s = \gamma_{\text{rf}} I'_s. \tag{89}$$

Substituting Eq. (88) into Eq. (89) gives the total anode current in the *LFR* provided by n (59) electron spokes as

$$I_a = \varepsilon_0 \upsilon_{\text{rf}} \gamma_{\text{rf}} n \frac{2E_{\text{rf}} \sinh(pr_L)}{1-\alpha\gamma_{\text{rf}}^2} \frac{\pi L_z}{p2r_L}. \tag{90}$$

Substituting Eqs. (19) and (48) into Eq. (90) gives the total anode current in the "zero-order magnitude" approximation for the π mode of a relativistic magnetron operation:

$$I_a = \varepsilon_0 \upsilon_{\mathrm{rf}} \gamma_{\mathrm{rf}} n \frac{4E_0}{\pi} \frac{\sin(ha)}{\sinh(pd)} \frac{\sinh(pr_L)}{1-\alpha\gamma_{\mathrm{rf}}^2} \frac{\pi L_z}{p2r_L} = \varepsilon_0 \upsilon_{\mathrm{rf}} \gamma_{\mathrm{rf}} 2NE_0 \frac{\sin(ha)}{\sinh(pd)} \frac{\sinh(pr_L)}{1-\alpha\gamma_{\mathrm{rf}}^2} \frac{L_z}{pr_L}. \tag{91}$$

Finally, the following parameters are needed to analytically calculate the anode current of a relativistic magnetron operating in the π mode (91): cathode r_c and anode r_a radii, width a and number N of cavities, cathode length L_z, frequency f of the π mode, external dc AK voltage V_0, and magnetic field H_0. One needs also to define the effective radius r_e, where the drift velocity of an electron υ_{dc} (27) is compared with the phase velocity of the traveling rf wave υ_{rf} (20), specifying in this way the detuning coefficient α (32). It can be either anode r_a or cathode r_c or middle r_m radii, supposing that r_e does not depend on the AK voltage U_0 and the magnetic field H_0, or it can be equal to the Larmor diameter $2r_L$, supposing that r_e is a function of the AK voltage U_0 and the magnetic field H_0.

3. Comparison of Analysis and Simulations

There are a number of approximations adopted to develop the analytic theory allowing one to calculate, among all other important characteristics of a relativistic magnetron operation, the anode current (91): (1) the "planar-geometry-magnetron" approximation (51) and (52) used to represent the cylindrical geometry of a multicavity magnetron by its planar analog; (2) the "zero-order-magnitude" approximation (48) postulating that the induced rf electric field $E_{\sim}$ amplitude E_1 (7) equals the external dc electric field $E_{\perp}$ amplitude E_0 (8a); (3) the "guiding-center-motion" approximation (80) used to represent the complex trajectory of an electron moving between the anode and the cathode (electron drift in the crossed electric and magnetic fields and electron gyration in the magnetic field) by a trajectory of the drifting egcon only; and (4) the "zero-space-charge" approximation used to determine drift velocities υ_x' (73) and υ_y' (79) of electrons between the cathode and the anode without accounting for the self-space charge of the drifted electrons.

The validity of using the "planar-geometry-magnetron" approximation (51) and (52) is examined by parameter R (Ref. 7) that defines the "cylindricity" of a magnetron:

$$R = r_a/r_c. \tag{92}$$

It was shown in Ref. 7 that "the characteristics of cylindrical magnetron with $R < 2.273$ differ very little from the planar characteristics and the difference can be ignored for most practical purposes." Given the geometrical dimensions of the "classical" A6 relativistic magnetron, $r_c = 1.58$ cm and $r_a = 2.11$ cm, its parameter of cylindricity R is 1.33, which does allow one to approximate this magnetron by its planar model. The validity of using all other approximations can be examined at this point only by analyzing and checking the analytically calculated anode current (91), lettered hereafter as I_a^{cal}, against the anode current obtained either in PIC simulations of the magnetron operation, lettered hereafter as I_a^{sim}, or during the experimental measurements on this magnetron, lettered hereafter as I_a^{exp}.

Below is the comparison, I_a^{cal} against I_a^{sim}, of anode currents of the A6 relativistic magnetron operating in the π mode. Comparison is made for the applied AK voltage 350 kV, as a typical voltage of the magnetron operation, as well as for some other

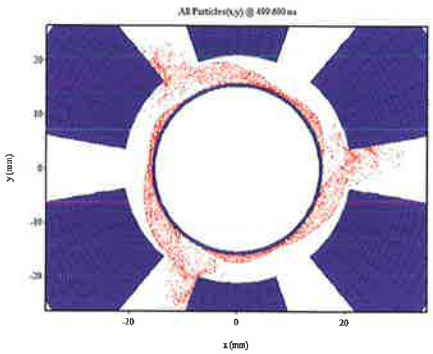

Fig. 12. Particle plot corresponding to the π mode of A6 relativistic magnetron operation at $V_0 = 350$ kV, $B_0 = 0.72$ T.

voltages being of interest for either experimental or computer exercises. All simulations are performed using the commercially available PIC code MAGIC.†

3.1. 2D PIC simulations of A6 relativistic magnetron at applied voltage 350 kV

PIC simulations of A6 magnetron operation for the applied AK voltage 350 kV are performed across the broad range of magnetic fluxes, 0.5–0.85 T, with a step of 0.01 T. The applied AK voltage rise time, from 0 to 350 kV, is 0.25 ns (instant turn-on voltage); the magnetic flux is uniform and perpendicular to the simulation plane determined in the cylindrical 2D (r–θ) geometry. Total simulation time is 500 ns, which allows the magnetron to assuredly achieve a steady-state regime of operation where I_a^{sim} can be compared with I_a^{cal}.

Simulations show that the π mode of magnetron oscillation occurs only in a limited range of magnetic fluxes, from 0.65 to 0.79 T; only those simulations that resulted in the clear π mode of the magnetron operation are analyzed below. The π mode is recognized by its characteristic three-spoke electron flow spatial distribution between the cathode and the anode; one can see in Fig. 12 a characteristic snapshot of the electron flow spatial distribution in the A6 magnetron obtained at magnetic flux 0.72 T. Beyond the magnetic field range allowing the π mode of the magnetron oscillations to exist, the electron flow spatial distribution is either chaotic or corresponds to some other modes of the magnetron operation (Fig. 13).

The following output characteristics of the PIC simulations are analyzed: (1) the AK voltage as a control parameter determining external dc electric field E_0 (8a) between the anode and the cathode, (2) the anode current I_a^{sim} in the steady-state regime of the magnetron operation as a parameter to be compared with the I_a^{cal} (91) anode current, (3) the rf voltage oscillations inside one of the six resonators of the magnetron, and (4) the frequency of these rf voltage oscillations as one of a few input parameters used for calculations I_a^{cal} (91). All these characteristics are shown in Fig. 14 in the time interval from 0 to 100 ns. The obtained I_a^{sim} [Fig. 14(b)] anode current is averaged in the time interval from 50 to 500 ns, in which

†http://www.magictoolsuite.com/.

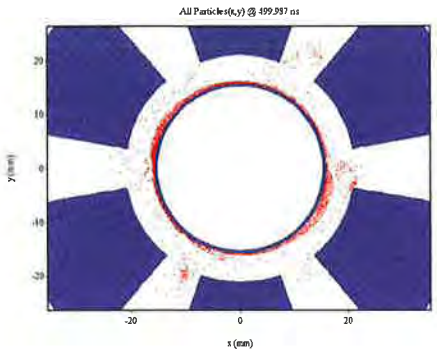

Fig. 13. Particle plot corresponding to some other, non–π mode of A6 relativistic magnetron operation at $V_0 = 350$ kV, $B_0 = 1.01$ T.

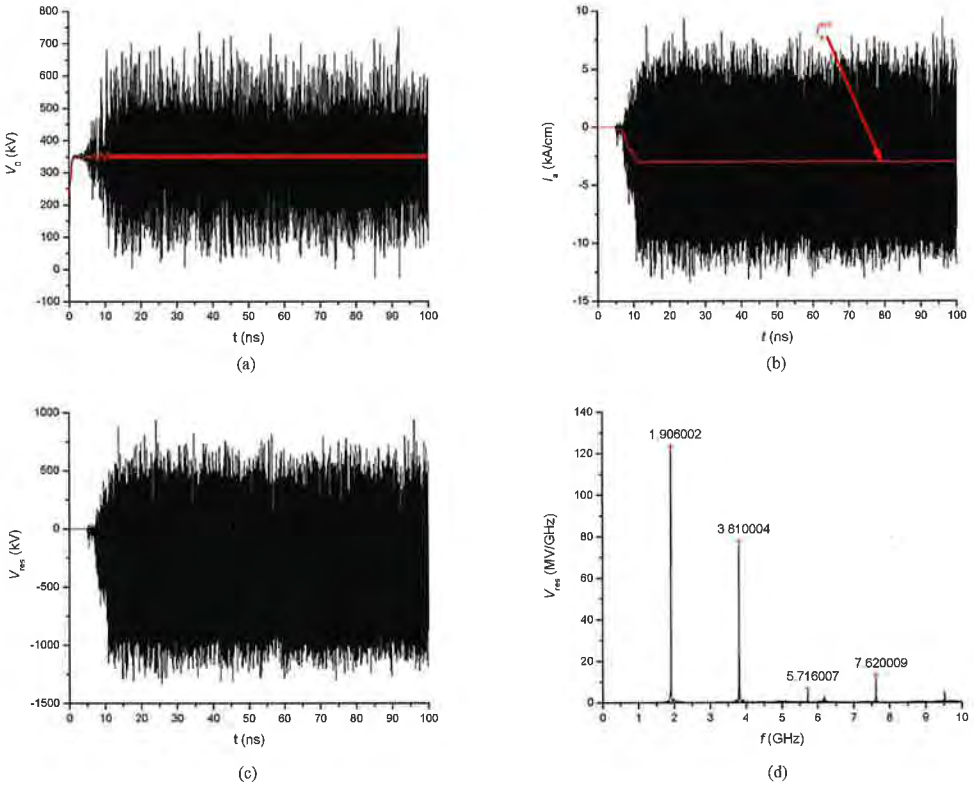

Fig. 14. Characteristic traces of A6 relativistic magnetron operating in the π mode at $V_0 = 350$ kV and $B_0 = 0.72$ T: (a) AK voltage oscillations, (b) I_a^{sim} anode current, (c) rf voltage in a resonator, and (d) frequency spectrum of rf voltage in a resonator.

the steady-state regime of the magnetron operation occurs, and compared with the I_a^{cal} (91) anode current; both currents are normalized to the unit length of a cathode.

The averaged I_a^{sim} anode current is plotted in Fig. 15 against four different I_a^{cal} (91) anode currents calculated using four different assumptions introduced in Section 2.4 to define the

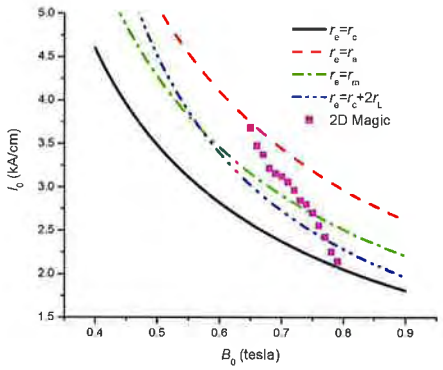

Fig. 15. Anode current of the A6 relativistic magnetron at AK voltage 350 kV vs. magnetic field: I_a^{cal} dependences are shown by solid lines; I_a^{sim} dependence is shown by points.

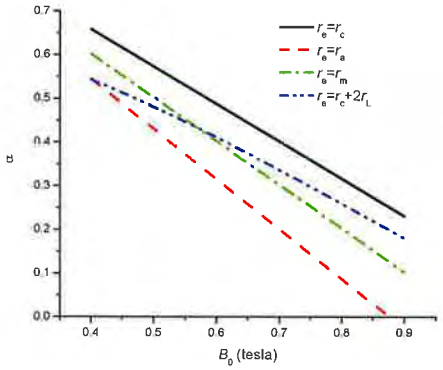

Fig. 16. Detuning coefficient α (32) corresponding to four different I_a^{cal} of the A6 relativistic magnetron; AK voltage is 350 kV.

effective radius r_e (53), (55)–(57), which, in its turn, determines (i) the length of one spatial period of the planar magnetron D (52), (ii) the longitudinal wave number h (21), (iii) the phase velocity of the traveling rf wave (20), and, finally, (iv) the detuning coefficient α (32). The appropriate values of the detuning coefficient α (32) are shown in Fig. 16.

One can see in Fig. 15 that the averaged I_a^{sim} anode current decreases from ~3.75 to ~2.25 kA/cm as the magnetic flux increases from 0.65 to 0.79 T. Analyzing this result against the calculated dependencies of the detuning coefficient α (Fig. 16) shows that the π mode of the magnetron oscillation (Fig. 12) occurs only at positive values of the detuning coefficient α (32), when the drift velocity υ_{dc} (27) of an electron at the "boundary line" x_b (33) is somewhat higher than the phase velocity of the traveling rf wave υ_{rf} (20). The π mode of the magnetron oscillation does not exist (Fig. 13) even at the exact synchronism determining by condition (31), $\alpha = 0$. This is another evidence of the well-known fact that the magnetron oscillations can grow and be sustained only when the drift velocity of electrons in the crossed dc electric and magnetic fields υ_{dc} (27) is somewhat higher than the phase velocity of the traveling rf wave υ_{rf} (20) (Ref. 37, p. 311, Fig. 62; Ref. 9, pp. 219–220, Fig. 7–17).

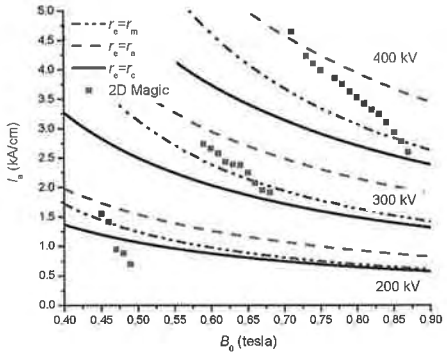

Fig. 17. Anode current of the A6 relativistic magnetron at three different AK voltages vs. magnetic field: I_a^{cal} dependences are shown by solid lines; I_a^{sim} dependence is shown by points.

Comparison of the I_a^{sim} anode current against the I_a^{cal} (Fig. 15) anode current shows that all values of the I_a^{sim} anode current are confined in between two limiting I_a^{cal} anode currents calculated using (i) the assumption (55), $r_e = r_a$, as a higher limit of the I_a^{cal} anode current and (ii) the assumption (56), $r_e = r_c$, as a lower limit of the I_a^{cal} anode current. The maximum value of the I_a^{sim} anode current is close to the I_a^{cal} anode current calculated using assumption (55), i.e., at maximum thickness of the electron sheath, $2r_L = r_a - r_c$. The minimum value of the I_a^{sim} anode current corresponds to the I_a^{cal} anode current calculated using assumption (56), i.e., at a minimum thickness of the electron sheath, $r_L \sim 0$. This result shows that the limiting values of the I_a^{sim} anode current correspond to two limiting conditions of the electron sheath formation when, in one limit, the electron sheath occupies all the distance between the cathode and the anode and, in the other limit, the electron sheath thickness is close to zero.

Comparison of the I_a^{cal} anode current against the I_a^{sim} anode current (Fig. 15) shows also that the I_a^{sim} anode current is determined by the effective radius r_e variation between the cathode and the anode that follows the magnetic field H_0 variation. However, the dependence of the I_a^{cal} anode current on the magnetic field H_0, when it is calculated using assumption (57), $r_e = r_c + 2r_L$, which models the electron sheath thickness variation with the magnetic field H_0 change as the appropriate variation of the Larmor diameter (60), does not correspond to the I_a^{sim} anode current dependence on the magnetic field H_0. This result shows that the thickness of the electron sheath determining the I_a^{sim} anode current dependence on the magnetic field H_0 is rather complicated and cannot be approximated by the appropriate dependence of the Larmor diameter (60).

3.2. 2D PIC simulations of A6 relativistic magnetron at other voltages of interest

The averaged I_a^{sim} obtained from PIC simulations ($V_0 = 200$, 300, and 400 kV) is compared in Fig. 17 against three different I_a^{cal} (91) anode currents calculated using three different assumptions defining the effective radius r_e (55)–(57), when at the given AK voltage V_0, the effective radius r_e (i) equals the anode radius r_a (Ref. 34, p. 1350), in accordance with (55), (ii) equals the cathode radius r_c, in accordance with (56), or (iii)

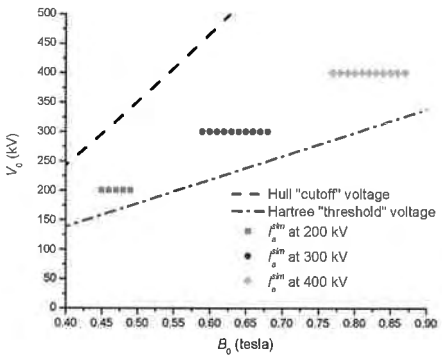

Fig. 18. Hull cutoff and Buneman–Hartree voltages and operating voltages from PIC simulations of the A6 relativistic magnetron that operates in π mode (1.95 GHz) vs. magnetic field.

varies with the magnetic field B_0 variation as described by (57), in accordance with (53). The averaged I_a^{sim} anode currents are plotted also on the magnetic flux–applied voltage ($B_0 - V_0$) parameter space (Fig. 18) showing the A6 magnetron operating domain bounded by the Hull "cutoff" [Ref. 6, p. 272, Eq. (7.5)] and Hartree "threshold" [Ref. 6, p. 273, Eq. (7.8)] voltages. The PIC simulation of the A6 magnetron operations at these AK voltages is done by the same manner as it is at the AK voltage 350 kV.

Comparison of the I_a^{sim} anode current against the I_a^{cal} anode current (Fig. 17) shows that the I_a^{sim} anode current obtained at $V_0 = 300$ and 400 kV is also confined between two limiting I_a^{cal} anode currents as it is at $V_0 = 350$ kV (Fig. 15). The dependence of the anode current I_a^{sim} obtained at $V_0 = 200$ kV is different; only those I_a^{sim} anode currents that are obtained at lower magnetic fields, $B_0 = 0.45$–0.46 T, are confined within the two limiting I_a^{cal} anode currents, whereas the I_a^{sim} anode current obtained at higher magnetic fields is less than the I_a^{cal} anode current calculated using assumption (56), i.e., at the minimum thickness of the electron sheath, $r_L \sim 0$. This result does not say, of course, that at these specific operating parameters of the A6 magnetron, $V_0 = 200$ kV and $B_0 = 0.47$–0.49 T, the effective radius r_e is becoming less than the cathode radius r_c. This result shows that in this particular case either (i) some approximations adopted to develop the analytic theory of a relativistic magnetron operations are invalid or (ii) some peculiarities of the magnetron operation associated with this specific region on the $B_0 - V_0$ parameter space, which are not included in the analytic theory applied for calculating anode current (91), affect the anode current formation or (iii) this purely computational effect is introduced by this particular PIC code.

Placement of the A6 magnetron operating parameters at which the π mode (Fig. 12) of magnetron operation exists on the $B_0 - V_0$ parameter space (Fig. 18) shows that all these operating points (B_0, V_0) are situated between the Hull "cutoff" [Ref. 6, p. 272, Eq. (7.5)] and Hartree "threshold" [Ref. 6, p. 273, Eq. (7.8)] voltages. This is another evidence of the well-known fact that the magnetron oscillations can grow and be sustained only when, at the given AK voltage V_0, (i) the drift velocity of electrons in the crossed dc electric and magnetic fields υ_{dc} (27) is somewhat higher than the phase velocity of the traveling rf wave υ_{rf} (20) (Ref. 37, p. 311, Fig. 62; Ref. 9, pp. 219–220, Fig. 7–17), which is the Hartree "threshold" voltage [Ref. 6, p. 273, Eq. (7.8)], and (ii) the Larmor diameter of electrons in

the applied magnetic field H_0 is less that the AK spacing, which is the Hull "cutoff" voltage [Ref. 6, p. 272, Eq. (7.5)].

One can see also that the I_a^{sim} anode current dependence is determined by the electron sheath thickness variation in the magnetic field as it is at $V_0 = 350$ kV. The electron sheath thickness dependence on the external dc AK voltage V_0 and the magnetic field H_0 is, however, much more complicated than the Larmor radius dependence on the magnetic field.

4. Conclusions

The analytical expression for calculation of anode current in a relativistic magnetron is derived [Eq. (91)]. The anode current is described as the cathode-to-anode drift of the electron guiding centers (egcons) in the crossed dc and induced rf electric and magnetic fields. To derive the expression for the anode current, the cylindrical geometry of a magnetron is approximated by its planar equivalent and the drift of the electron guiding centers is analyzed in the moving frame of reference that moves with a velocity equal to the phase velocity of the traveling rf wave associated with the induced rf electric field. The drift of the electron guiding centers from the cathode to the anode is analyzed using the "zero-space-charge" and the "zero-order-magnitude" approximations. The anode current determined by this drift is calculated under an assumption that the cathode operates in a space-charge-limited mode, when the external dc electric field at the cathode surface is zero.

Results of the analytical calculations of the anode current of the A6 relativistic magnetron are compared with PIC computer simulations of the anode current of the "classical" A6 relativistic magnetron operating in the π mode. The PIC simulations are performed using the 2D MAGIC code. The analytical calculations are done using four different assumptions used to define the effective cathode radius r_e determining the length of one spatial period of the planar magnetron D and the longitudinal wave number when (1) r_e equals the cathode radius, (2) r_e equals the anode radius, (3) r_e is in the geometrical center between the cathode and the anode, and (4) r_e decreases with the magnetic field increase as described by the Larmor diameter dependence on the magnetic field.

Analysis of the results and comparison of the analytically calculated anode current and the anode current obtained in the PIC simulations shows that, at the reasonably high applied AK voltage $V_0 > 250$ kV, the I_a^{sim} anode current varies with the magnetic field variation from its maximum value at the minimum magnetic field, allowing the π mode of magnetron oscillations to exist, to its minimum value at the maximum magnetic field, allowing the π mode of the magnetron oscillations to exist. Both maximum and minimum values of the anode current obtained in the PIC simulations correspond to the analytically calculated anode current at a given applied AK voltage and a given magnetic field, obtained when the r_e radius equals the anode radius and when the r_e radius equals the cathode radius, respectively. The character of the I_a^{sim} anode current dependence on the magnetic field is, however, different from the character of the I_a^{cal} anode current dependence on the magnetic field, when the latter one is analytically calculated assuming that the electron sheath thickness changes with the magnetic field as the Larmor diameter does. This result shows that the variation of the anode current obtained in the PIC simulations does depend on the electron sheath thickness but the latter parameter has more complicated dependence on the magnetic field than the Larmor radius.

5. Appendix: Magnetic Field Components of the Induced rf Field

5.1. Nonrelativistic field components

The induced rf magnetic field $H_{\sim}$ can be obtained from the appropriate $E_{\sim}$ field using the following relation [Ref. 17, p. 66, Eq. (26.1)]:

$$\nabla \times E = -\mu_0 \frac{\partial H}{\partial t}, \tag{A.1}$$

Taking into account that there are the $E_{\sim x}$ and the $E_{\sim y}$ fields (11), the only $H_{\sim z}$ field can be defined using Eq. (A.1):

$$-\mu_0 \frac{\partial H_{\sim z}}{\partial t} = \frac{\partial E_{\sim y}}{\partial x} - \frac{\partial E_{\sim x}}{\partial y}. \tag{A.2}$$

Substituting Eq. (11) into Eq. (A.2) gives

$$-\mu_0 \frac{\partial H_{\sim z}}{\partial t} = \frac{\partial}{\partial x}[-E_1 \cosh(g_\perp y)\sin(g_\parallel x - \omega t)] - \frac{\partial}{\partial y}[-E_1 \sinh(g_\perp y)\cos(g_\parallel x - \omega t)],$$

$$\mu_0 \frac{\partial H_{\sim z}}{\partial t} = E_1 g_\parallel \cosh(g_\perp y)\cos(g_\parallel x - \omega t) - E_1 g_\perp \cosh(g_\perp y)\cos(g_\parallel x - \omega t),$$

$$-\mu_0 \frac{\partial H_{\sim z}}{\partial t} = E_1(g_\parallel - g_\perp)\cosh(g_\perp y)\cos(g_\parallel x - \omega t), \tag{A.3}$$

or, taking into account Eq. (5), i.e., that $g_\perp = g_\parallel$,

$$\mu_0 \frac{\partial H_{\sim z}}{\partial t} = 0. \tag{A.4}$$

Thus, in accordance with Eq. (A.4), there is no $H_{\sim}$ field, which was implicitly supposed by Kapitsa, when he considered only the $E_{\sim}$ field (9) and, of course, both $E_\perp$ and $H_\perp$ fields (8), in his planar magnetron.[16]

5.2. Relativistic field components

The induced rf magnetic field $H_{\sim}$ can also be obtained from the appropriate $E_{\sim}$ field using Eq. (A.3). Substituting Eqs. (18a) and (18b) into Eq. (A.2) gives

$$-\mu_0 \frac{\partial H_{\sim z}}{\partial t} = E_1 \frac{\partial}{\partial x}[\sinh(px)\cos(hy - \omega t)] - \frac{\partial}{\partial y}\left[\frac{h}{p}\cosh(px)\sin(hy - \omega t)\right],$$

$$-\mu_0 \frac{\partial H_{\sim z}}{\partial t} = E_1 p \cosh(px)\cos(hy - \omega t) - \frac{h}{p} h \cosh(px)\cos(hy - \omega)), \; -\mu_0 \frac{\partial H_{\sim z}}{\partial t}$$

$$= E_1 \left(p - \frac{h^2}{p}\right)\cosh(px)\cos(hy - \omega t) = E_1 \frac{p^2 - h^2}{p}\cosh(px)\cos(hy - \omega t). \tag{A.5}$$

Substituting $k^2 = h^2 - p^2$ [Eq. (23)] into Eq. (A.5) gives

$$-\mu_0 \frac{\partial H_{\sim z}}{\partial t} = -E_1 \frac{k^2}{p}\cosh(px)\cos(hy - \omega t). \tag{A.6}$$

Integrating Eq. (A.6) gives

$$-\mu_0 \int^{\partial} H_{\sim z} = -\int_1^E \frac{k^2}{p} \cosh(px) \cos(hy - \omega t),$$

$$-\mu_0 H_{\sim z} = E_1 \frac{k^2}{p} \cosh(px) \frac{-\sin(hy - \omega t)}{-\omega}, \tag{A.7}$$

$$H_{\sim z} = E_1 \frac{k}{\mu_0 \omega} \frac{k}{p} \cosh(px) \sin(hy - \omega t),$$

and substituting $k = \omega c = \omega\sqrt{\mu_0 \varepsilon_0}$ [Eq. (16)] into Eq. (A.7) gives

$$H_{\sim z} = E_1 \frac{\omega\sqrt{\mu_0 \varepsilon_0}}{\mu_0 \omega} \frac{k}{p} \cosh(px) \sin(hy - \omega t) = E_1 \frac{1}{\sqrt{\mu_0/\varepsilon_0}} \frac{k}{p} \cosh(px) \sin(hy - \omega t). \tag{A.8}$$

Taking into account the fact that, as it follows from Eq. (23),

$$\frac{k}{p} = \beta_{\mathrm{rf}} \gamma_{\mathrm{rf}}, \tag{A.9}$$

one can rewrite Eq. (A.8) using $k/p = \gamma_{\mathrm{rf}} \beta_{\mathrm{rf}}$ [Eq. (23)] as

$$H_{\sim z} = E_1 \frac{\beta_{\mathrm{rf}} \gamma_{\mathrm{rf}}}{\sqrt{\mu_0/\varepsilon_0}} \cosh(px) \sin(hy - \omega t) = E_1 \frac{k}{c\mu_0 p} \cosh(px) \sin(hy - \omega t). \tag{A.10}$$

One can see now that Eq. (A.10) corresponds to Eq. (18c).

In the nonrelativistic case, $\gamma_{\mathrm{rf}} \to 1$ and and $\beta_{\mathrm{rf}} \to 0$, the $H_{\sim}$ field [Eqs. (A.8) and (A.10)] vanishes to zero.

The fields and drifts are summarized in Table A.1.

Table A.1. Summary of the fields and drifts

	LFR	MFR	MFR at $\alpha = 0$, when $\beta_{dc} = \beta_{rf}$
External dc electric field, $E_{\perp x}$	$-E_0$	$-\alpha\gamma_{rf}E_0$	0
External dc magnetic field, $H_{\perp z}$	H_0	$H_0\frac{\beta_{dc}}{\gamma_{rf}\beta_{rf}}\left(1-\alpha\gamma_{rf}^2\right)$	$\frac{H_0}{\gamma_{rf}}$
Induced rf electric field, $E_{\sim y}$	$E_1\sinh(py)\cos(hx-\omega t)$	$E_1\sinh(px)\cos(py')$	$E_1\sinh(px)\cos(py')$
Induced rf electric field, $E_{\sim x}$	$\frac{h}{p}E_1\cosh(py)\sin(hx-\omega t)$	$E_1\cosh(px)\sin(py')$	$E_1\cosh(px)\sin(py')$
Induced rf magnetic field, $H_{\sim z}$	$\frac{1}{\sqrt{\mu_0/\varepsilon_0}}\frac{k}{p}E_1\cosh(px)\sin(hy-\omega t)$	0	0
Drift velocity in the EMF^{dc}, υ_{dc}	$\frac{E_0}{\mu_0 H_0}$	$\gamma_{rf}^2\beta_{rf}\frac{\alpha}{1-\alpha\gamma_{rf}^2}$	0
Larmor radius, r_L	$c^2\beta_{dc}^2\frac{m_e}{\lvert q_e\rvert E_0}$	$\frac{\lvert-\upsilon_{rf}+\upsilon'_{dc}\rvert c\gamma_{rf}^2\beta_{rf}}{1-\alpha\gamma_{rf}^2}\frac{m_e}{q_eE_0}$	$c^2\beta_{rf}^2\gamma_{rf}^2\frac{m_e}{q_eE_0}$
Cyclotron frequency, ω_c	$\frac{\lvert q_e\rvert E_0}{m_e\upsilon_{dc}}$	$\frac{\lvert q_e\rvert}{m_e\gamma_{rf}}\mu_0H_0\frac{\beta_{dc}}{\gamma_{rf}\beta_{rf}}\left(1-\alpha\gamma_{rf}^2\right)$	$\frac{\lvert q_e\rvert}{m_e\gamma_{rf}^2}\mu_0H_0$

References

[1]Barker, R.J., and E. Schamiloglu (Eds.), "Relativistic Magnetrons," in *High-Power Microwave Source and Technologies*, IEEE Press Series on RF and Microwave Technology, p. 56 (2001).

[2]Bekefi, G., and T.J. Orzechowski, "Microwave Emission from Magnetically Insulated Relativistic Electron-Beam Diodes," Proceedings of the IEEE International Pulsed Power Conference, Lubbock, TX, November 9–11, 1976, p. IIC6-1 (1976).

[3]Bekefi, G., and T.J. Orzechowski, Phys. Rev. Lett. **37**(6), 379 (1976).

[4]Benford, J., "Relativistic Magnetrons," in *High-Power Microwave Sources*, edited by V.L. Granatstein and I. Alexeff, Artech House, p. 351 (1987).

[5]Benford, J., and J. Swegle, "Cross-Field Devices," in *High-Power Microwaves*, Artech House, p. 147 (1992).

[6]Benford, J., J.A. Swegle, and E. Schamiloglu, "Relativistic Magnetrons and MILOs," in *High-Power Microwaves*, 2nd Ed. Taylor & Francis Group, p. 259 (2007).

[7]Brillouin, L., and F. Bloch, Adv. Electronics **3**, 145 (1951).

[8]Bronshtein, I.N., and K.A. Semendyayev, *Handbook of Mathematics*, English translation edited by K.A. Hirsch, Van Nostrand Reinhold Company, New York (1985).

[9]Chan, H.W., C. Chen, and R.C. Davidson, J. Appl. Phys. **73**(11), 7053 (1993).

[10]Chen, F.F., *Introduction to Plasma Physics*, Plenum Press, New York (1974).

[11]Collins, G.B. *Microwave Magnetrons*, McGraw-Hill (1948).

[12]Davidson, R.C., *An Introduction to the Physics of Nonneutral Plasmas*, Addison-Wesley (1990).

[13]Davidson, R.C., H.W. Chan, C. Chen, and S. Lund, Rev. Modern Phys. **63**(2), 341 (1991).

[14]Fuks, M.I., "Study of Electron Flows in Systems with Magnetic Insulation," Dissertation written as a part of the work toward the Degree of the Candidate to Physical-Mathematical Sciences, Institute of Applied Physics, USSR Academy of Sciences, Gorkiy (1983).

[15]Hok, G., and W.G. Dow, "Principles of Magnetron Operation," in *Very High-Frequency Techniques*, compiled by the staff of the Radio Research Laboratory of Harvard University and edited by H.J. Reich, McGraw-Hill Book Company, Volume I (1947).

[16]Kapitza, P.L., *High-Power Microwave Electronics*, translated from the Russian by S. and M. Nikolic, Pergamon Press (1964).

[17]Landau, L.D., and Lifshitz, E.M. *The Classical Theory of Fields,* Fourth Revised English Edition, translated from the Russian by M. Hamermesh, Pergamon Press (1975).

[18]Miller, R.B., "The Relativistic Microwave Magnetron," in *An Introduction to the Physics of Intense Charged Particle Beams*, Plenum Press, p. 214 (1982).

[19]Nechajev, V.E., Izvestiia Vysshikh Uhebnykh Zavedenii Radiophysika **5**(3), 534 (1962).

[20]Nechajev, V.E., Izvestiia Vysshikh Uhebnykh Zavedenii Radiophysika **5**(3), 1035 (1962).

[21]Nechajev, V.E., M.I. Petelin, and M.I. Fuks, Sov. Tech. Phys. Lett. **3**(8), 310 (1977).

[22]Nechaev, V.E., A.S. Sulakshin, M.I. Fuks, and Yu. G. Shtein, "Relativistic Magnetron," in *Relativistic High-Frequency Electronics, Proceedings of All-Union (USSR) Conference, Gorkiy, 26–28 September, 1978*, Institute of Applied Physics, USSR Academy of Sciences, p. 114 (1979).

[23]Nusinovich, G.S., T.M. Antonsen, Jr., V.L. Bratman, and N.S. Ginzburg, "Principles and Capabilities of High-Power Microwave Generators," in *Application of High-Power Microwaves*, edited by A.V. Gaponov-Grekhov and V.L. Granatstein, Artech House, p. 25 (1994).

[24]Okress, E. (Ed.), *Crossed-Field Microwave Devices*, Academic Press (1961).

[25]Orzechowski, T.J., and G. Bekefi, Phys. Fluids **19**(1), 43 (1976).

[26]Palevsky, A., and G. Bekefi, Phys. Fluids **22**(5), 986 (1979).

[27]Reintjes, J.F., and G.T. Coate (Eds.), "Klystrons and Magnetrons," in *Principles of Radar*, compiled by the staff of the Radar School of the Massachusetts Institute of Technology, McGraw-Hill Book Company (1952).

[28]Riyopoulos, S., Phys. Fluids B **3**(12), 3505 (1991).

[29]Riyopoulos, S., J. Plasma Phys. **46**(3), 473 (1991).

[30]Riyopoulos, S., IEEE Trans. Plasma Sci. **20**(3), 360 (1992).

[31]Riyopoulos, S., Phys. Rev. E **47**(4), 2839 (1993).

[32]Riyopoulos, S., Phys. Plasmas **3**(3), 1137 (1996).

[33]Riyopoulos, S., IEEE Trans. Plasma Sci. **26**(3), 755 (1998).

[34]Riyopoulos, S., Phys. Plasmas **6**(4), 1144 (1999).

[35]Riyopoulos, S., D.P. Chernin, and A.T. Drobot, IEEE Trans. Electron Devices **39**(6), 1529 (1992).

[36]Schwartz, M., *Principles of Electrodynamics, International Series in Pure and Applied Physics,* L.I. Schiff, Consulting Editor, McGraw-Hill Book Company (1972).

[37]Slater, J.C., "The Magnetron Oscillator," in *Microwave Electronics*, D. Van Nostrand Company (1950).
[38]Tsimring, S.E., "Relativistic Magnetrons," in *Electron Beams and Microwave Vacuum Electronics*, Wiley, p. 400 (2007).
[39]Vainshtein, L.A., and V.A. Solntsev, *Lectures on Very-High-Frequency Electronics*, Soviet Radio (1973).

The Authors

Dr. Andrey D. Andreev enrolled in the Physics Department of the Tomsk State University (TSU) in 1983 and subsequently received the Diploma of Physics with a major in plasma physics in 1990. During his study at the TSU, he worked in the Theoretical Laboratory of the High-Current Electronics Institute, Tomsk, USSR/Russia (HCEI), where he gained a strong theoretical background and research computer simulation experience in the physics of charge-particle beam generation, formation, transportation, and interaction with matter. In 1993, he joined the Laboratory of the High-Current Pulsed Accelerators (NIL SIU) of the Efremov Institute of Electrophysical Apparatus, St. Petersburg, Russia (NIIEFA), and spent 10 years there doing experimental and calculational science and technique of high-current, microsecond-duration electron-beam accelerators with explosive-emission multipoint cathodes. From January 2003 to December 2007, he pursued his graduate education at the Department of Electrical and Computer Engineering of the University of New Mexico (UNM), where he studied all aspects of microwave engineering, plasma physics, antenna theory, computational techniques, etc., while working in the Laboratory of the Pulsed Power Beams, Microwaves and Plasmas of the UNM as a Research Assistant. Since the beginning of 2008, he has been a NRC Associate at the Air Force Research Laboratory, Directed Energy Directorate, High Power Microwave Division (AFRL/RDHPS). His research interests include high-power microwave generation, relativistic and nonrelativistic magnetron operation, high-power microwave antennas, applied electromagnetics and metamaterials, and plasma physics. He is a member of the IEEE, the American Physical Society, the Directed Energy Professional Society (DEPS), and the Sigma Xi Research Society.

Dr. Mikhail I. Fuks received the Ph.D. degree in physical electronics from the Institute of Applied Physics (IAP), Russian Academy of Sciences, Nizhny Novgorod. In 1963, he joined the Gorky Radio-Physical Research Institute, Nizhny Novgorod. In 1977, he joined IAP, working in the field of high-power microwave electronics as a Scientist and then as a Senior Scientist and as the Head of a research group. In 1999, he traveled to the United States to work in radar technology sponsored by the Ballistic Missile Defense Organization. Since 2000, he has been with the Electrical and Computer Engineering Department, University of New Mexico, Albuquerque, as a Research Professor. His current research interests include the formation and transportation of electron beams, the development and application of various types of high-power microwave sources, and electrodynamics systems. Dr. Fuks is a member of the American Physical Society.

Dr. Kyle J. Hendricks received the B.S. and M.S. degrees in physics from the University of Iowa, Iowa City, in 1980 and 1982, respectively, and the Ph.D. degree from the University of New Mexico, Albuquerque, in 1989. Since 1983, his research interests have included narrow-band, high-power-microwave (HPM) sources, electron beam diodes and propagation, pulsed power systems, laboratory plasma systems, and diagnostic techniques for laboratory plasmas and HPM systems. Dr. Hendricks received the 1988 U. S. Air Force (USAF) Research and Development Award and was a corecipient of the 2001 Directed Energy Giller Award and the 2001 USAF Science and Engineering Award.

Dr. Edl Schamiloglu received the B.S. and M.S. degrees from the School of Engineering and Applied Science, Columbia University, New York, in 1979 and 1981, respectively, and the Ph.D. degree in applied physics (minor in mathematics) from Cornell University, Ithaca, New York, in 1988. He joined the University of New Mexico as an Assistant Professor in 1988, and he is currently Gardner-Zemke Professor of Electrical and Computer Engineering. He coedited *Advances in High Power Microwave Sources and Technologies* (IEEE, Piscataway, NJ, 2001) (with R.J. Barker), and he coauthored *High Power Microwaves*, 2nd ed. (Taylor & Francis, New York, 2007) (with J. Benford and J. Swegle). He is a Senior Editor of the *IEEE Transactions on Plasma Science* and an Associate Editor of the *Journal of Electromagnetic Waves and Applications*. He has been actively researching HPM sources for more than 20 years. He is a Fellow of the IEEE and an EMP Fellow of the Summa Foundation.